A&A 576, A79 (2015)
DOI: 10.1051/0004-6361/201423829

Astronomy & Astrophysics

The VIMOS Ultra-Deep Survey: ~10 000 galaxies with spectroscopic redshifts to study galaxy assembly at early epochs $2 < z \simeq 6$★,★★

O. Le Fèvre[1], L. A. M. Tasca[1], P. Cassata[1], B. Garilli[3], V. Le Brun[1], D. Maccagni[3], L. Pentericci[4], R. Thomas[1], E. Vanzella[2], G. Zamorani[2], E. Zucca[2], R. Amorin[4], S. Bardelli[2], P. Capak[12], L. Cassarà[3], M. Castellano[4], A. Cimatti[5], J. G. Cuby[1], O. Cucciati[5,2], S. de la Torre[1], A. Durkalec[1], A. Fontana[4], M. Giavalisco[13], A. Grazian[4], N. P. Hathi[1], O. Ilbert[1], B. C. Lemaux[1], C. Moreau[1], S. Paltani[9], B. Ribeiro[1], M. Salvato[14], D. Schaerer[10,8], M. Scodeggio[3], V. Sommariva[5,4], M. Talia[5], Y. Taniguchi[15], L. Tresse[1], D. Vergani[6,2], P. W. Wang[1], S. Charlot[7], T. Contini[8], S. Fotopoulou[9], C. López-Sanjuan[11], Y. Mellier[7], and N. Scoville[12]

[1] Aix-Marseille Université, CNRS, LAM (Laboratoire d'Astrophysique de Marseille) UMR 7326, 13388 Marseille, France
e-mail: olivier.lefevre@lam.fr
[2] INAF–Osservatorio Astronomico di Bologna, via Ranzani,1, 40127 Bologna, Italy
[3] INAF–IASF, via Bassini 15, 20133 Milano, Italy
[4] INAF–Osservatorio Astronomico di Roma, via di Frascati 33, 00040 Monte Porzio Catone, Italy
[5] University of Bologna, Department of Physics and Astronomy (DIFA), V.le Berti Pichat, 6/2 – 40127 Bologna, Italy
[6] INAF–IASF Bologna, via Gobetti 101, 40129 Bologna, Italy
[7] Institut d'Astrophysique de Paris, UMR 7095 CNRS, Université Pierre et Marie Curie, 98bis boulevard Arago, 75014 Paris, France
[8] Institut de Recherche en Astrophysique et Planétologie – IRAP, CNRS, Université de Toulouse, UPS-OMP, 14 avenue E. Belin, 31400 Toulouse, France
[9] Department of Astronomy, University of Geneva, Ch. d'Écogia 16, 1290 Versoix, Switzerland
[10] Geneva Observatory, University of Geneva, Ch. des Maillettes 51, 1290 Versoix, Switzerland
[11] Centro de Estudios de Física del Cosmos de Aragón, 44001 Teruel, Spain
[12] Department of Astronomy, California Institute of Technology, 1200 E. California Blvd., MC 249–17, Pasadena, CA 91125, USA
[13] Astronomy Department, University of Massachusetts, Amherst, MA 01003, USA
[14] Max-Planck-Institut für Extraterrestrische Physik, Postfach 1312, 85741 Garching bei München, Germany
[15] Research Center for Space and Cosmic Evolution, Ehime University, Bunkyo-cho 2-5, 790-8577 Matsuyama, Japan

Received 18 March 2014 / Accepted 7 January 2015

ABSTRACT

We present the VIMOS Ultra Deep Survey (VUDS), a spectroscopic redshift survey of ~10 000 very faint galaxies to study the main phase of galaxy assembly in $2 < z \simeq 6$. The survey covers 1 deg^2 in three separate fields: COSMOS, ECDFS, and VVDS-02h, with the selection of targets based on an inclusive combination of photometric redshifts and colour properties. Spectra covering $3650 < \lambda < 9350$ Å are obtained with VIMOS on the ESO-VLT with integration times of 14h. Here we present the survey strategy, target selection, data processing, and the redshift measurement process with an emphasis on the specific methods used to adapt to this high-redshift range. We discuss the spectra quality and redshift reliability and derive a success rate in redshift measurement of 91%, or 74% by limiting the dataset to the most reliable measurements, down to a limiting magnitude $i_{AB} = 25$. Measurements are performed all the way down to $i_{AB} = 27$. The mean redshift of the main sample is $z \sim 3$ and extends over a broad redshift range mainly in $2 < z < 6$. At $3 < z < 5$, the galaxies cover a wide range of luminosities $-23 < M_{NUV} < -20.5$, stellar mass $10^9\ M_\odot < M_* < 10^{11}\ M_\odot$, and star formation rates $1\ M_\odot/\mathrm{yr} < SFR < 10^3\ M_\odot/\mathrm{yr}$. We discuss the spectral properties of galaxies using individual as well as stacked spectra. The comparison between spectroscopic and photometric redshifts as well as colour selection demonstrate the effectiveness of our selection scheme. From about ~90% of the data analysed so far, we expect to assemble >6000 galaxies with reliable spectroscopic redshifts in $2 < z < 6$ when complete. This makes the VUDS the largest survey at these redshifts and offers the opportunity for unprecedented studies of the star-forming galaxy population and its distribution in large-scale structures during the main phase of galaxy assembly.

Key words. galaxies: evolution – galaxies: high-redshift – cosmology: observations – large-scale structure of Universe – surveys – galaxies: formation

1. Introduction

The study of the first billion years of galaxy evolution is one of the key frontiers of modern cosmology. The current theoretical paradigm rests on the hierarchical build-up of dark matter halos in a ΛCDM cosmology (see e.g. Mo et al. 2010). Galaxies that formed in these deep potential wells are expected to transform primordial gas into stars from the initial reservoir and are thought to be fed from new accreted gas. As dark matter halos merge, galaxies in them are also expected to merge, which events deeply transform the dynamics and overall stellar, gas, and dark matter content of the merging galaxies into the newly formed one. Complex processes

★ Based on data obtained with the European Southern Observatory Very Large Telescope, Paranal, Chile, under Large Program 185.A-0791.
★★ Staged releases of the data will appear on http://cesam.lam.fr/vuds/, starting in mid-2015.

are invoked to regulate the growth of galaxies, including supernovae or AGN feedback that possibly quenches star formation, or the role of different environments that affect the way galaxies are nurtured. Increasingly sophisticated galaxy simulations in representative volumes (e.g. Springel et al. 2008) coupled to semi-analytic description of galaxy evolution (e.g. Guo et al. 2011) need better constraints from observations to be thoroughly tested.

Impressive progress has been made on the observational front over the past two decades in an attempt to test and detail a galaxy formation and evolution scenario from reliable measurements. A key element driving observational progress is the need to cover all main phases of galaxy evolution from the early formation and galaxy assembly to today – a formidable endeavour. Deep galaxy surveys have flourished to conduct this exploration. The latest few billion years have been extensively mapped by surveys like the 2dFGRS (Colless et al. 2001) and from the various stages of the SDSS (Abazajian et al. 2009), setting a firm observational reference after more than 13 billion years of evolution. At higher redshifts, deep surveys are providing a complex picture with strong evolutionary features such as the build-up of stellar mass in galaxies of different types during cosmic time, or the star formation history. Imaging and spectroscopic surveys play a complementary role, the deepest studies being performed in photometry and augmented with photometric redshifts (e.g. Ilbert et al. 2006; Rix et al. 2004; Guo et al. 2011; Koekemoer et al. 2007, 2011), and with spectroscopic surveys bringing accurate redshifts and spectro-photometry, spectral features properties, and internal velocity information. Fundamental quantities have been measured from these surveys including the cosmic star formation history (e.g. Lilly et al. 1996; Madau et al. 1996; Tresse et al. 2007; Cucciati et al. 2012; Madau & Dickinson 2014), and the history of stellar mass assembly (e.g. Arnouts et al. 2007; Ilbert et al. 2013).

At redshifts $z \sim 1$, the pioneering CFRS survey (Lilly et al. 1995; Le Fèvre et al. 1995) was followed by more extensive galaxy redshift surveys covering larger volumes, such as the DEEP2 (Davis et al. 2003), the VVDS (Le Fèvre et al. 2005b, 2013a), and zCOSMOS (Lilly et al. 2007), which now reaches the 100 000 redshift mark at $z \sim 1$ with VIPERS (Guzzo et al. 2014). These surveys have brought a wealth of quantitative and accurate measurements now in large enough areas of a few tens of sq. deg and volumes of $\sim 5 \times 10^7\, h^{-3}\,\mathrm{Mpc}^3$ so that the most fundamental statistical quantities describing the galaxy population, such as the luminosity function (LF), the mass function (MF), or the correlation function (CF), are becoming very accurate and less affected by the cosmic variance related to the small fields of earlier studies. At higher redshifts ($z > \sim 2$), the rapid progress has been driven by the effectiveness in selecting high-redshift galaxies and, most importantly, by the impressive gains in sensitivity and efficiency provided by high multiplex multi-slit spectrographs such as DEIMOS (Faber et al. 2003) on the Keck telescope and VIMOS (Le Fèvre et al. 2003) on the VLT. The effectiveness of the Lyman-break galaxies (LBG) selection has provided the capability of finding large numbers of galaxies at $z > 2.5$ (e.g. Steidel et al. 2003; Bouwens et al. 2009; Ellis et al. 2013). It is supplemented by narrow-band imaging techniques isolating Lyman-α emitters (LAE; Taniguchi et al. 2005; Shimasaku et al. 2006; Ouchi et al. 2008). In addition to these pre-selection techniques, deep purely magnitude-selected surveys are conducted to probe a large population mostly free of pre-selection biases. At redshifts $z > 1.5$, the largest magnitude-selected survey is currently the VVDS which covers up to $z \sim 6.5$ (Le Fèvre et al. 2005b, 2013b). Other magnitude-selected surveys have attempted to use redder bands to prevent from selecting only galaxies with strong rest-frame UV continuum. The K20 survey used K-band magnitude selection down to $K = 20$ to identify extremely red objects (EROs) at $z \sim 1.5$–2 (Cimatti et al. 2002), and the GMASS survey selected objects on the basis of *Spitzer* near-IR photometry with $m_{4.5\ \mu\mathrm{m}} < 23.0$ (AB) to identify a few hundred galaxies with $1.5 < z < 3$ (Cimatti et al. 2008). However, and despite these successful studies, the approach using pure magnitude selection is costly in observing time when going much beyond a redshift of $z \sim 2$.

Performing a complete galaxy census is a basic astronomy input necessary for any subsequent astrophysical analysis. While at redshifts $\sim$1 this census is mostly complete down to stellar mass $10^8\ M_\odot$, this is not yet the case at redshifts $z > 1$ for several reasons. First, the colour-selection schemes applied to photometric samples to extract the high-redshift populations are efficient in identifying galaxies, but are affected by significant incompleteness, loosing some fraction of the population at the selected redshift, or by contamination from galaxies at other redshifts. While the latter can be dealt with by obtaining spectroscopic redshifts, the former remains a serious difficulty especially at faint magnitudes and at the highest redshifts. Unfortunately, the level of incompleteness strongly depends on the photometric filters used for imaging, the depth of the observations, and the image quality, and estimating this incompleteness requires a case-by-case study that involves source simulations. These are further complicated by the need to make a priori hypotheses on the properties of galaxies one is trying to establish. It was realised that a colour–colour selection such as the LBG technique at $z > 2.5$ or the BzK, which works at $z \simeq 2$ (Daddi et al. 2004), would miss a part of the general galaxy population in their selection process (Le Fèvre et al. 2005a), which would cause the galaxy census to be incomplete (Le Fèvre et al. 2013a). The consequences of this may be far-reaching, as incompleteness in counts leads to underestimates in luminosity density, star formation rates, or mass density, to cite just a few consequences. An important aspect of on-going and future studies is to revisit galaxy counts as a function of redshift, ensuring that no significant population is missing and that no significant bias is introduced in deriving astrophysical quantities.

A key element for this is the availability of large samples of galaxies with a well-defined and well-controlled selection function. Spectroscopic redshift surveys play a key role because they provide samples with confirmed redshifts. Photometric redshift surveys are widely used and have now reached an impressive accuracy. The level of "catastrophic failures" when photometric redshifts disagree with their training set of spectroscopic redshifts, even if low at a few percent (Ilbert et al. 2013), could still produce large unknowns, however, because of the shape of the redshift distribution $N(z)$ of flux limited samples. An error of 1% at the peak, $z \simeq 1$, of the $N(z)$ of a $i_{\mathrm{AB}} = 25$ sample could spread galaxies with incorrect photometric redshifts to higher redshifts, for instance at $z \sim 3$, where the projected galaxy density is lower than ten times the $N(z)$ at peak, which represents several tens of percent of uncertainty. One recent example is the difficulty of distinguishing $z \sim 5$ very massive objects from lower redshift lower mass $z \sim 2$ galaxies (Wiklind et al. 2008; Caputi et al. 2012). Obtaining a spectroscopic redshift therefore remains a fundamental measurement.

The total number of galaxies spectroscopically confirmed today at $z > 2$ is still limited. Published LBG samples reach $\sim$2000 redshifts at $z \sim 3$, only a few hundred at $z \sim 4$, and several tens of galaxies beyond that (Steidel et al. 2003; Vanzella et al. 2009; Stark et al. 2010; Bielby et al. 2013). Samples of

Table 1. VUDS fields.

Field	α_{2000}	δ_{2000}	b	l	Area	Depth
COSMOS	10h00m04.0s	+02°12′40″	42.1	236.8	1800 arcmin^2	$i_{AB} \simeq 25$
ECDFS	03h32m28.0s	−27°48′30″	−54.0	223.5	675 arcmin^2	$i_{AB} \simeq 25$
VVDS-02h	02h26m00.0s	−04°30′00″	−57.5	172.0	1125 arcmin^2	$i_{AB} \simeq 25$

LAE galaxies selected with narrow-band techniques and confirmed in spectroscopy reach a few hundred objects beyond $z = 3$ (Ouchi et al. 2008; Kashikawa et al. 2011). The high-redshift tail of the VVDS at $z > 2$ contains about 1000 galaxies (Le Fèvre et al. 2013a). To overcome the uncertainties linked to small existing spectroscopic samples and to understand the biases and limitations of photometry-based studies in their ability to provide a complete census of the galaxy population, extremely deep spectroscopic surveys over large volumes are needed.

Here we present VUDS, the VIMOS Ultra Deep Survey that is specifically designed to study the early phases of galaxy evolution in $2 < z < 6+$ from ∼10 000 targeted galaxies. The VUDS sample contains an unprecedented number of galaxies with secure spectroscopic redshifts at this epoch, obtained in three different fields: COSMOS, ECDFS, and VVDS-02h. The survey design, including the target selection, is based mainly on photometric redshifts, as presented in Sect. 2. The VIMOS multi-slit spectroscopic observations, data reduction, and redshift measurement scheme are discussed in Sect. 3. Properties of the VUDS sample are presented in Sect. 4, including the redshift distribution of the sample, the distribution of intrinsic properties such as stellar mass and star formation rate, and the average spectra properties based on stacked spectra with a high signal-to-noise ratio (S/N). After comparing to other surveys in Sect. 5, we summarize our results in Sect. 6 and conclude that the VUDS survey will be very useful to study the early phases of galaxy assembly with unprecedented accuracy.

All magnitudes are given in the AB system unless specified, and we use a cosmology with $\Omega_M = 0.3$, $\Omega_\Lambda = 0.7$, and $h = 0.7$.

2. Survey design

2.1. Science drivers

When the VUDS survey observing-time proposal was approved at the end of 2009, spectroscopic redshift surveys were still of limited scope at the epoch of galaxy assembly significantly beyond redshifts $z \sim 2$–3. The VUDS survey therefore aimed to address several core science goals at the epoch $2 < z < 6+$, including (i) the early history of the global star formation rate; (ii) the build-up of the mass function for different galaxy populations, and the contribution to mass assembly and star formation of merging, feedback, and accretion; (iii) the study of very young galaxies in their early stages of assembly, including the earliest stellar populations like Pop III; (iv) the identification of proto-structures and the effects of environment at early stages of galaxy evolution; and (v) the study of the clustering of galaxies to infer the mass growth of underlying dark matter halos.

These broad science goals still remain hot science topics today and are the main focus of VUDS.

2.2. Survey strategy overview

The VUDS survey is designed to study the galaxy population beyond redshift $z \simeq 2$ and up to the highest redshifts possible in the wavelength range up to $\lambda = 9350$ Å that is accessible with the VIMOS spectrograph on the VLT (see below); it corresponds to Lyα at a redshift up to $z \simeq 6.6$. A total of one sq. deg is observed in three well-separated fields to mitigate cosmic variance effects: the COSMOS field, the extended *Chandra* Deep Field South (ECDFS), and the VVDS-02h field. This program was awarded Large Program status with 640 h of VLT-VIMOS observing time.

A key feature of the survey is the target selection. It is primarily based on photometric redshifts and their probability distribution function (PDF), complemented by colour–colour selections and analysis of the shape of the spectral energy distribution (SED) when not already in the photo-z selection. When the geometry of the observed slit-masks allows it after placing the previous priority targets, a purely magnitude-selected random sample of galaxies with $23 \leq i_{AB} \leq 25$ has been added to the target list. This is further described in Sect. 2.5.

The second key feature is the extended wavelength coverage of the VIMOS spectroscopic observations covering $3650 \leq \lambda \leq 9350$ Å, which minimizes any instrument-induced redshift desert and strongly reduces the degeneracies in redshift measurements Le Fèvre et al. (2013b).

The last key point is the integration time of ≃14 h per target, which allows reaching a S/N on the continuum at 8500 Å of $S/N = 5$ for $i_{AB} = 25$, and $S/N = 5$ for an emission line with a flux $F = 1.5 \times 10^{-18}$ erg/s/cm^2/Å.

2.3. Survey fields

VUDS covers three of the most frequently observed extragalactic fields: the COSMOS field, the ECDFS, and the VVDS-02h (also known as the CFHTLS-D1/XMM-LSS field). A total of 0.5 sq. deg are observed in the COSMOS field, 0.31 sq. deg in the VVDS-02h field, and 0.14 sq. deg in the ECDFS. The field locations and area each field covers are summarized in Table 1 and identified in Figs. 1 to 3.

2.4. Multi-wavelength data and photometric catalogues

By design, the three survey fields accumulate a wealth of deep multi-wavelength data and spectroscopy. This is an important part of VUDS because multi-wavelength coverage of the SED is essential in combination with accurate spectroscopic redshifts, in particular to derive key physical quantities such as absolute magnitudes, stellar masses, and star formation rates or ages. We describe the most relevant existing data for each field. We note that when the spectroscopic targets were selected over the 2010–2012 period, we used the datasets available at the time as an input to the selection function. The physical parameters derived from multi-wavelength photometry reported here (e.g. stellar mass $M_\star$ and star formation rate) and in other VUDS studies make use of the latest datasets available.

The COSMOS field (Scoville et al. 2007) is extensively observed at all wavelengths. Its location was set up close to one of

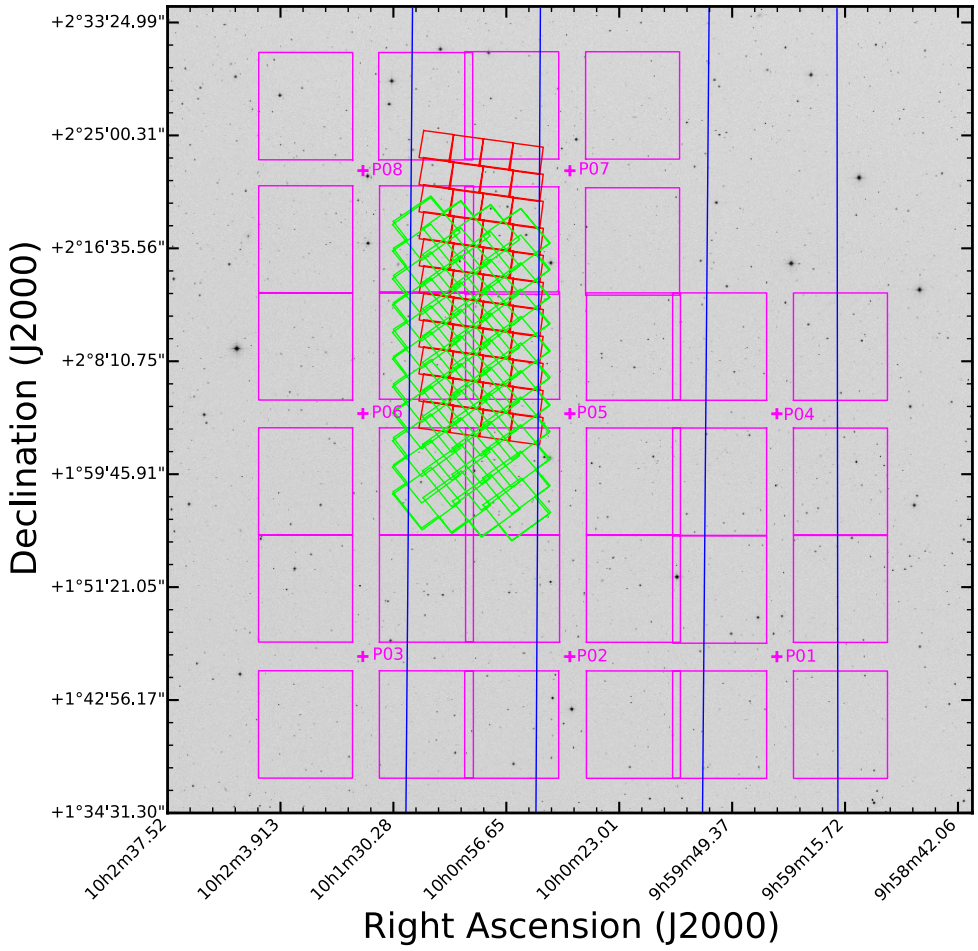

Fig. 1. Layout of the observed 8 VUDS VIMOS pointings in the COSMOS field. The centre of each VIMOS pointing is identified by a cross with the pointing number (see Table 3), while the imprint of the 4 quadrants is plotted in magenta. The positions of the UltraVista Deep stripes overlapping with the VUDS area are identified by the blue regions. The CANDELS ACS-*F814W* (in green) and WFC3-*F160W* (in red) areas are indicated. The size of the image is 1×1 deg^2.

the original VVDS fields, with the centre moved to a region with lower galactic extinction when better extinction maps became available. The field was observed with HST-ACS in the *F814W* filter (Koekemoer et al. 2007), providing high spatial resolution imaging down to a depth AB($F814W$) = 27.2 (5σ). Extensive imaging observations were obtained in g, r, i, and z bands from the Subaru SuprimeCam (Taniguchi et al. 2007) and from the CFHT Megacam from the CFHT-Legacy Survey, which includes the u-band, and photometry is available from 12 medium bands (references available in Ilbert et al. 2009). The UltraVista survey is acquiring very deep near-IR imaging in the Y, J, H, and K bands using the VIRCAM camera on the VISTA telescope (McCracken et al. 2012). The UltraVista DR2 release reaches a depth of $K_{\rm AB} = 24.8$ at 5σ (in 2 arcsec apertures), and it is planned to increase the depth down to $K_{\rm AB} = 25.5$ in half the area by the end of the survey. The VUDS VIMOS pointings are placed in a way to optimize the overlap with the deeper UltraVista stripes (Fig. 1). Following the initial *Spitzer* observations (Sanders et al. 2007), deeper *Spitzer*-warm observations are obtained by the Splash program, reaching AB = 25.4 (5σ at 3.6 μm) (Capak et al., in prep.) with a smaller area on one UltraVista stripe observed from the SEDS survey, which pushes down to AB = 26 at 3σ (Ashby et al. 2013). The COSMOS field has deep *Herschel* imaging reaching 8 mJy at 250 μm (Oliver et al. 2012). The CANDELS survey (Grogin et al. 2011) in this field includes WFC3 imaging in the *F125W* (J) and *F160W* (H) filters down to $H_{\rm AB} = 27.1$ (5σ); the CANDELS area is almost entirely covered by the VUDS pointings (Fig. 1).

Extensive spectroscopy was obtained in the COSMOS field before VUDS. The zCOSMOS survey (Lilly et al. 2007) contains 20 000 galaxies with $0 < z < 1.2$ selected with $i_{\rm AB} \leq 22.5$ and ~6000 galaxies selected with $g_{\rm AB} \simeq 25$–25.5 with $1.4 < z < 3$ and a median redshift $z = 2.15$ (Lilly et al., in prep.). Deep spectroscopy from Keck has identified several hundred galaxies in the same redshift range as VUDS (e.g. Capak et al. 2011). VUDS targeting avoided re-observing those galaxies with existing reliable redshifts, when known. A wealth of observations at other wavelengths are available in this field; we refer to the COSMOS web site[1] for the detailed list and properties.

The ECDFS field is the focus of a number of deep multi-wavelength surveys. Built around the field with deep 1Ms *Chandra* observations (Giacconi et al. 2002), the field was extended and is covered with deep *UBVRI* imaging down to $R_{\rm AB} = 25.3$ (5σ, Cardamone et al. 2010 and references therein). Several spectroscopic surveys have been conducted (Le Fèvre et al. 2004b; Cardamone et al. 2010; Cooper et al. 2012) with more than 5000 galaxies with redshifts $0 < z < 2$, but the number of spectroscopically confirmed galaxies at $z > 2$ remains small. The central part of this field accumulates a number of deep HST imaging with the HDF-South (Williams et al. 2000), GEMS (Rix et al. 2004), and ERS (Windhorst et al. 2011) surveys, and more recently with the CANDELS survey (Grogin et al. 2011), which adds WFC3 near-IR imaging that reaches as deep as $H_{\rm AB} = 27.3$–27.6. The SERVS *Spitzer*-warm obtained

[1] http://cosmos.astro.caltech.edu/

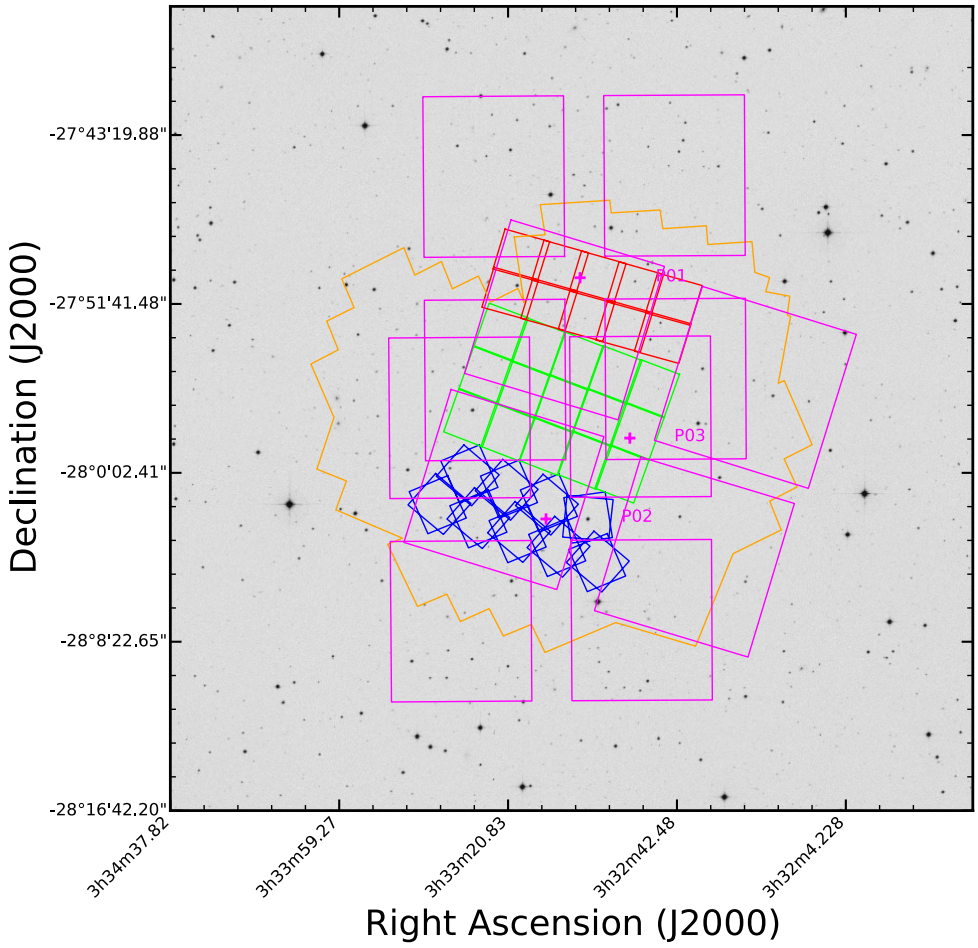

Fig. 2. Layout of the observed 3 VUDS VIMOS pointings in the ECDFS field. The centre of each VIMOS pointing is identified by a cross with the pointing number (see Table 3), while the imprint of the 4 quadrants is plotted in magenta. The positions of the CANDELS WFC3 deep area is indicated in green, the CANDELS wide area in blue. The red region indicates the WFC3 coverage of the ERS. The outline of the existing ACS-*F814W* imaging is identified in orange. The size of the image is 0.67×0.67 deg^2.

3.6 and 4.5 μm imaging data down to AB = 23.1 (Mauduit et al. 2012).

The VVDS-02h field was originally defined as the "deep field" of the VVDS survey. It was observed in *BVRI* at CFHT (Le Fèvre et al. 2004a), followed by deeper u', g, r, i observations as the D1 deep field in the CFHTLS survey reached $i_{\rm AB}$ = 25.44 at 50% completeness in the latest DR7 (Cuillandre et al. 2012). Deep infrared imaging was obtained with the WIRCAM at CFHT in *YJHK* bands down to $Ks_{\rm AB}$ = 24.8 also at 50% completeness (Bielby et al. 2012). Extensive multi-slit spectroscopy was obtained with VIMOS as the "Deep" and "Ultra-Deep" surveys of the VVDS, with magnitude-selected samples down to $I_{\rm AB}$ = 24 and $i_{\rm AB}$ = 24.75, respectively. A total of 11 139 objects have spectroscopic redshift measurements from the VVDS, including 774 with $z > 2$. This field was observed in all *Spitzer* bands as part of the SWIRE survey (Lonsdale et al. 2003), reaching a magnitude in the 3.6 microns band of AB = 21.5. More recently, the SERVS survey obtained deeper data with *Spitzer* in the 3.6 μm and 4.5 μm bands down to AB = 23.1 at 3.6 μm (Mauduit et al. 2012). It is one of the fields of the HERMES survey (Oliver et al. 2012), that matches CFHTLS and VVDS data (Lemaux et al. 2014b). A number of other deep data are available, including X-ray (Pierre et al. 2004) and radio (Bondi et al. 2003) observations.

In each field, photometric catalogues including data at least from the u-band to the *Spitzer* 4.5 μm band have been assembled, matching the different imaging sources, and extracting photometry in 2 arcsec apertures in dual mode using SExtractor (Bertin & Arnouts 1996). On the COSMOS field we used the photometric catalogues published by the COSMOS collaboration (see e.g. a full description of the u-band to 4.5 μm catalogues in the context of the UltraVista survey, Ilbert et al. 2013. In the VVDS-02h field we used the CFHTLS photometry for u-band to z-band (Cuillandre et al. 2012) and the WIRDS photometry for *YJHK* (Bielby et al. 2012), PSF-matched. In these two fields, the source detection was performed using χ^2 images resulting from a combination of images from u-band to z-band. In the ECDFS field we used the catalogues assembled by (Cardamone et al. 2010), and we refer to this paper for the details on its construction.

2.5. Spectroscopic target selection

As shown from the VVDS, the redshift distribution of faint galaxies, for example down to $i_{\rm AB} \simeq 25$, is peaked at $z \sim 1.3$–1.5, with a rapidly decreasing high-redshift tail (Le Fèvre et al. 2013a). Magnitude selection is therefore inefficient in picking-up $z > 2$ galaxies among the far more numerous foreground. This prompted the use of the Lyman-break selection technique, as pioneered by Steidel and collaborators (Steidel et al. 1996) This technique makes simple use of the colour properties of galaxies as a function of redshift, identifying a locus in colour–colour space associated with specific redshift ranges.

A more sophisticated technique for pre-selecting high-redshift galaxies follows the development of the photometric redshift technique, and its demonstrated success in terms of the redshift measurement accuracy with typical errors of less than 5% on $\Delta z/(1+z)$ and a lower rate of catastrophic errors than spectroscopic redshifts (Ilbert et al. 2010; Cardamone et al. 2010). In

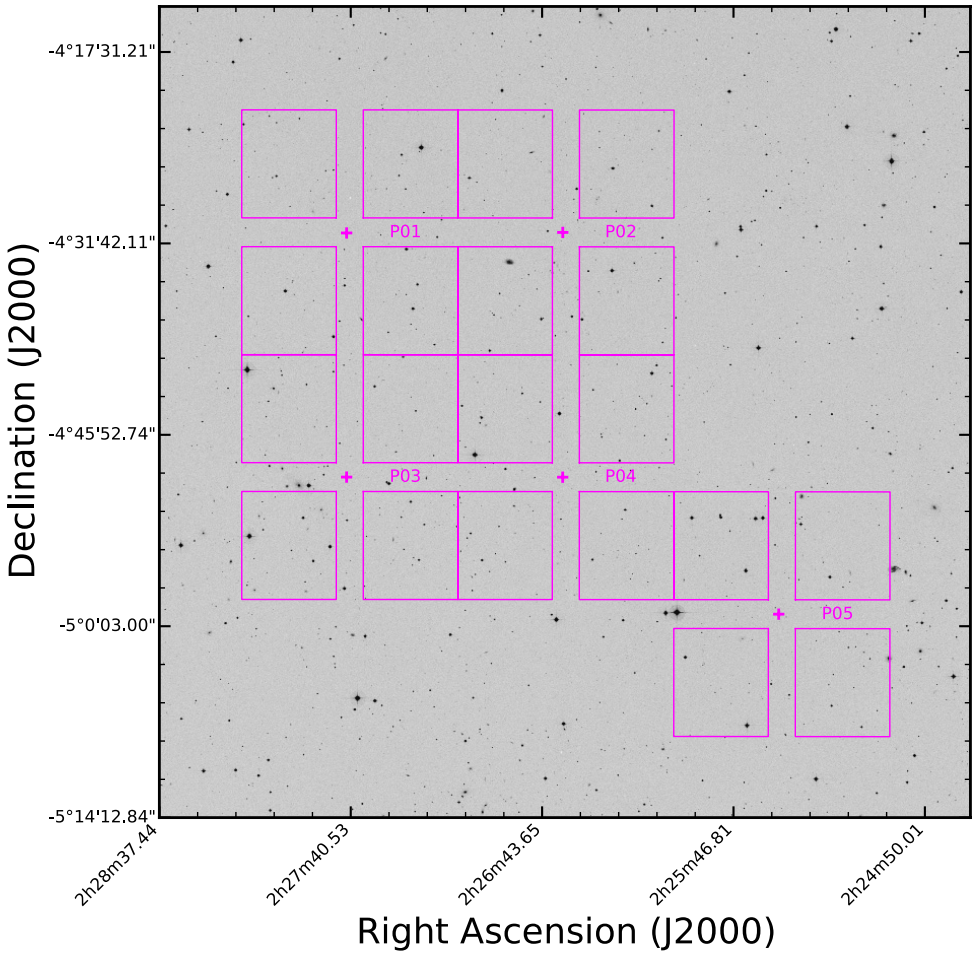

Fig. 3. Layout of the observed 5 VUDS VIMOS pointings in the VVDS-02h field. The centre of each VIMOS pointing is identified by a cross with the pointing number (see Table 3), while the imprint of the 4 quadrants is plotted in magenta. The size of the image is 1×1 deg^2. All of the VIMOS pointings are covered by CFHTLS visible photometry and WIRDS near-infrared photometry.

essence, photometric redshift techniques are a generalisation of colour-selection techniques such as LBG or BzK to the complete SED, which must satisfy a colour distribution across wavelengths compatible with reference galaxy templates. We elected to use the best possible photometric redshifts as our main selection criterion to define spectroscopic targets. Photometric redshifts have been computed with the code Le Phare (Arnouts et al. 1999; Ilbert et al. 2006) using the multi-band photometric catalogues covering from the u-band to the *Spitzer* 4.5 μm band. The techniques are described in Ilbert et al. (2009) and more recently in Ilbert et al. (2013). The observed photometric data are correlated against 33 templates covering a range from early- to late-type galaxies of different ages, star formation histories, and metallicities, leaving the $E(B-V)$ extinction as a free parameter. Emission lines with a flux empirically computed from the UV continuum flux are added to the templates. The "best" redshift is assigned from the median of the marginalized redshift PDF.

To select the spectroscopic targets in VUDS, we followed an *inclusive* rather than exclusive strategy, adding pre-selected samples from several different criteria, as described below.

- The spectroscopic targets must satisfy $z_{\rm phot} + 1\sigma \geq 2.4$, and $i_{\rm AB} \leq 25$. Because degeneracies are known to occur, we selected sources for which either the first or the second peak in the photometric redshift PDF satisfy this criterion. This corresponds to 87.7% of our primary sample.
- Sources that were not selected from the primary $z_{\rm phot}$ criterion but satisfy one of the *ugr*, *gri*, or *riz* LBG colour–colour selection criteria were added to the target list; they represent 8.4% of the primary sample.
- The full SED over all filters available in *ugrizYJHK* was used to identify galaxies with a break in the continuum that were not identified by any of the $z_{\rm phot}$ or LBG criteria; akin to the dropout technique. These targest were allowed to have $K_{\rm AB} \leq 24$ and hence may not necessarily be brighter than $i_{\rm AB} = 25$. This added another 3.9% to the primary sample.
- Finally, when space on the slit mask was still available after the above selections, a random "secondary" sample of galaxies with $23 \leq i_{\rm AB} \leq 25$ was selected; this represents 11.5% of the total sample.

For the last half of the survey observations, priority for slit placement was given to the targets with $z_{\rm estimate} \geq 4$ to increase the number of objects at these redshifts in the final sample.

In adding these different selection criteria, we aimed at maximizing the pre-selection of objects above $z = 2.4$. Given the dispersion of photometric redshift errors, we expect the redshift distribution of VUDS sources to start rising at $z \simeq 2$. While the selection strategy described above might lead to an increase in the contamination from objects at lower redshifts, this contamination remains quite weak, as described in Sect. 4.1. For each of the targeted samples, slits were placed at random using the `vmmps` slit mask design software (Bottini et al. 2005) which provided a fair and representative sample of the general population.

These various selection criteria are summarized in Table 2. In addition to the magnitude-selected sample that was used as a filler in the slit-mask design, the targeted high-z sample was selected for 87.7% on the basis of photometric redshifts, with

Table 2. VUDS spectroscopic target selection criteria.

Criterion	Value	Limiting magnitude	Fraction of targets
Photometric redshift, first PDF peak	$z_{\rm phot} + 1\sigma \geq 2.4$	$22.5 \leq i_{\rm AB} \leq 25$	58.3%
Photometric redshift, second PDF peak	$z_{\rm phot} \geq 2.4$	$22.5 \leq i_{\rm AB} \leq 25$	19.3%
LBG *ugr*	$2.7 < z < 3.5$	$i_{\rm AB} \leq 25$	1.9%
LBG *gri*	$3.5 < z < 4.5$	$i_{\rm AB} \leq 25$	1.9%
LBG *riz*	$4.5 < z < 5.5$	$i_{\rm AB} \leq 25$	3.6%
Break SED-based	–	$K_{\rm AB} \leq 24$	3.5%
Magnitude-selected	–	$23 \leq i_{\rm AB} \leq 25$	11.5%

Table 3. VUDS: observed VIMOS fields.

Pointing	α_{2000}	δ_{2000}	Grism
COSMOS-P01	09h59m02.39s	+01°54′35.9″	LRBLUE & LRRED
COSMOS-P02	10h00m04.08s	+01°54′35.9″	LRBLUE & LRRED
COSMOS-P03	10h01m05.76s	+01°54′35.9″	LRBLUE & LRRED
COSMOS-P04	09h59m02.39s	+02°12′41.4″	LRBLUE & LRRED
COSMOS-P05	10h00m04.08s	+02°12′41.4″	LRBLUE & LRRED
COSMOS-P06	10h01m05.76s	+02°12′41.4″	LRBLUE & LRRED
COSMOS-P07	10h00m04.08s	+02°30′46.7″	LRBLUE & LRRED
COSMOS-P08	10h01m05.76s	+02°30′46.7″	LRBLUE & LRRED
ECDFS-P01	03h32m25.99s	−27°41′59.9″	LRBLUE & LRRED
ECDFS-P02	03h32m34.00s	−27°53′59.9″	LRBLUE & LRRED
ECDFS-P03[a]	03h32m15.00s	−27°49′59.9″	MR
VVDS02-P01	02h26m44.51s	−04°16′42.8″	LRBLUE & LRRED
VVDS02-P02	02h25m40.34s	−04°16′42.8″	LRBLUE & LRRED
VVDS02-P03	02h26m44.51s	−04°34′50.3″	LRBLUE & LRRED
VVDS02-P04	02h25m40.34s	−04°34′50.3″	LRBLUE & LRRED
VVDS02-P05	02h24m36.14s	−04°44′57.9″	LRBLUE & LRRED

Notes. [(a)] The ECDFS-P03 has been observed with a VIMOS PA = 70 deg on the sky.

65.9% from the first peak in the photometric redshift PDF, and ∼21.8% from the second peak. The remaining about 12.3% is made up of the galaxies satisfying standard LBG and dropout colour–colour selection. The selection of VUDS galaxies is well defined and well controlled because both the parent catalogues and selection criteria are well documented and can be easily reproduced; this will be extensively described in a forthcoming paper. We note here that the selection technique providing the largest number of sources is the photometric redshift technique. Only about 50% of our sample satisfy LBG criteria over the full redshift range; had we used the LBG selection alone, we would have missed ∼50% of the star-forming galaxy population. This can be easily understood from considering that the photometric redshift selection produces a continuous redshift distribution, while in each redshift range defined by any two colour filter set, the LBG selection produces a bell-shaped redshift distribution. This means that it misses an increasingly large fraction of sources at the redshift extremes of the redshift domain covered by a three-filter set when the continuum features produced by the Lyman limit and IGM absorption move through the three filters. When using several colour–colour selections to cover a wide redshift range (e.g. *ugr*, *gri*, *riz*) the redshift distribution from LBG selection is the sum of several of these bell-shaped functions (as seen e.g. in Bouwens et al. 2014, Fig. 1). While this incompleteness in photometric LBG samples is usually corrected for using simulations, LBG source selection as an input to spectroscopy over a wide redshift range $2 < z < \sim 6$ like in VUDS would then miss ∼50% of the possible targets from the onset. Our strategy of using photometric redshifts instead of LBG selection was designed to avoid this severe difficulty. The effect of our selection function and a comparison between the different selection criteria will be analysed in detail in a forthcoming paper.

3. Observations, data processing, and redshift measurement

3.1. VIMOS on the VLT

The VIsible Multi-Object Spectrograph (VIMOS) is installed on the European Southern Observatory Very Large Telescope unit 3 Melipal. VIMOS is a wide-field imaging multi-slit spectrograph (Le Fèvre et al. 2003) that offers broad-band imaging capabilities and multi-slit spectroscopy. VIMOS is a high-performance Multi-Object Spectrograph (MOS) with four parallel channels, each a complete imaging-spectrograph with a field of view of 8×7 arcmin^2, or a total field of 224 arcmin^2. The key features of VIMOS are a high multiplex (number of slits) and the excellent sky subtraction accuracy, which reaches $\sigma_{\rm sky\ residual} \simeq 0.1\%$ of the sky signal (Le Fèvre et al. 2013b).

For VUDS we used the low-resolution multi-slit mode of VIMOS; with the four channels, this offers the largest multiplex for multi-slit spectroscopy. Following Scodeggio et al. (2009), we optimized the slit length to allow for lengths as small as 6 arcsec, which in turn maximizes the number of observed slits.

3.2. VIMOS observations

We observed a total of 16 VIMOS pointings at the coordinates of the pointings identified in Table 3. Fifteen pointings are observed with both the LRBLUE grism covering $3650 \leq \lambda \leq 6800$ Å and the LRRED grism covering $5500 \leq \lambda \leq 9350$ Å, leading to a full wavelength coverage of $3650 \leq \lambda \leq 9350$ Å. With slits one arc-second wide, these grisms provide a spectral resolution $R = 230$ quite uniformly over the wavelength range. At this resolution, each of the four 2048×4096 pixels detectors can accommodate three to four full-length spectra along the dispersion direction, and given the projected space density of VUDS targets, we therefore observed on average $N_{\rm slits} \simeq 600$ individual slits simultaneously. Each slit may contain not only the VUDS pre-selected target, but also serendipitous objects falling in the slit by chance.

One pointing on the ECDFS (#3) was observed with the MR grating. This setup covers $5000 \leq \lambda \leq 9500$ Å with a spectral resolution $R = 580$. With this resolution, about two full-length spectra can be placed along the dispersion direction, and a total of ~220 objects were observed in this pointing. The targets for this pointing were optimized towards the highest redshifts $z > 4.5$; the improved resolution compared to the LR grisms in principle slightly facilitates identifying emission lines like Lyα between the OH sky emission features (but possibly at the expense of sensitivity on continuum measurements).

Most VUDS observations were obtained after the CCD detectors were upgraded in the middle of 2010. At that time, the original blue–sensitive thinned E2V CCDs were changed to red–optimized thick E2V CCDs in 2010 (Hammersley et al. 2010). The global VIMOS sensitivity at 9000 Å increased by ~×2, making it similar to the FORS2 sensitivity in the red with a field of view 4.8× larger, and significantly reducing the fringing above 8000 Å thanks to the thicker substrate.

To reach a total integration of 14h, each of the LRBLUE or LRRED grism observations consisted on average of 13 observing blocks (OBs) executed at the telescope. Each OB includes three spectroscopic exposures of 1250 to 1350 s obtained by dithering $-0.75, 0,$ and $+0.75$ arcsec along the slit. The OBs specify the observing conditions that must be met, including a seeing better than 1 arcsec, sky transparency set to "clear", airmass lower than 1.5, dark time with constraints on the moon phase, and distance from the field (lunar illumination 0.3 to 0.5, and distance to the observed field of more than 60–90 deg). Arc lamp and flat-field calibrations were obtained after each set of three OBs, and flux calibration on standard stars was performed in the standard ESO procedure. When ready, OBs were sent to the VLT-VIMOS service observing queue via the P2PP tool and were executed when the atmospheric and moon conditions are met.

3.3. Spectroscopic data processing, redshift measurement, and reliability flags

The spectroscopic data-processing followed the same general principles as defined for the VVDS (Le Fèvre et al. 2005b, 2013b). We summarize this process below and emphasize the specific data-processing steps that we followed for VUDS.

The general outline of the VUDS data processing follows what is now a standard for multi-slit spectroscopy. We used the VIPGI environment to process the spectra (Scodeggio et al. 2005). First the 40 individual 2D spectrograms coming from the 13 OBs for one of the LRBLUE or LRRED observations are extracted to find the location of the slit projection on the detector using the position expectated from the slit-mask design. Sky subtraction was performed with a low-order spline fit along the slit for each wavelength sampled. The sky-subtracted 2D spectrograms are combined with sigma clipping to produce a single stacked 2D spectrogram calibrated in wavelength and flux. The 2D spectrogram is collapsed along the dispersion direction to produce a slit profile in which objects are identified. The spectral trace of the target and other detected objects in a given slit are linked to the astrometric frame to identify the corresponding target in the parent photometric catalogue.

This processing was performed separately for each of the LRBLUE and LRRED observations. In the wavelength range of overlap $5500 \leq \lambda \leq 6800$ Å, the end spectra are the average of the LRBLUE and LRRED, accumulating about 28 h of observation. The 1D sky-corrected stacked spectra were extracted following the observed slit profile. They were fully calibrated both in wavelength and in flux using spectrophotometric standard stars. The 2D and 1D fully calibrated spectra were cross-matched per observed slit and joined to form spectra with full $3650 \leq \lambda \leq 9350$ Å wavelength coverage. In this process, additional objects can be detected in the slit, and subsequently, we extracted their 1D spectra. These objects are called "secondary detections", and a photometric counterpart is searched for in the photometric catalogue. If an object is found within less than one arcsecond from the spectral trace, the secondary spectrum identification is assigned the identifier of the object in the photometric catalogue. If no object is found in the photometric catalogue, the spectrum of the object is extracted and a new entry is produced in the catalogue with coordinates at the location corresponding to the trace of the object. It might happen that a single emission line is identified upon visual examination of the 2D spectrogram of a given slit, but not extracted by the automated procedure: these objects were flagged and then extracted manually. This procedure is particularly important for objects with single emission lines and no or very little detected continuum, which are often found to be Lyα emitters at high redshifts (e.g. Cassata et al. 2011a).

Upon comparison between the photometric magnitudes and the magnitudes derived from the calibrated spectra, we realized that the u-band part of the spectra (and to a lesser extent the g-band) was lacking photons at the ~40% (~15%) level. We proceeded to add three well-defined corrections to the spectra: (1) atmospheric absorption; (2) atmospheric refraction; and (3) Galactic extinction. The atmosphere absorbs photons depending on the airmass along the light path; this was corrected for using the prescription defined for the Paranal observatory in Patat et al. (2011). In addition, atmospheric refraction acts as a small prism before entering the telescope, spreading the incoming light into a spectrum with length depending on the airmass and paralactic angle, the angle of the slit to the zenithal angle. With slit-masks placed on sky objects using an r-band filter before spectroscopic observations and slits one arcsecond wide, this may introduce a significant loss of uv-blue photons that fall out of the slit. The Galactic extinction on distant sources also produces a chromatic correction, which was applied using the $E(B-V)$ maps of Schlegel et al. (1998). In this process we also proceeded to produce spectra with continuum flux, which were calibrated on the i-band photometric flux; this corrects for any slit losses occurring in that band if the object extension is larger than the slit width.

By adding these corrections, we were able to correct the uv-blue spectroscopic flux in such a way that spectroscopic flux and

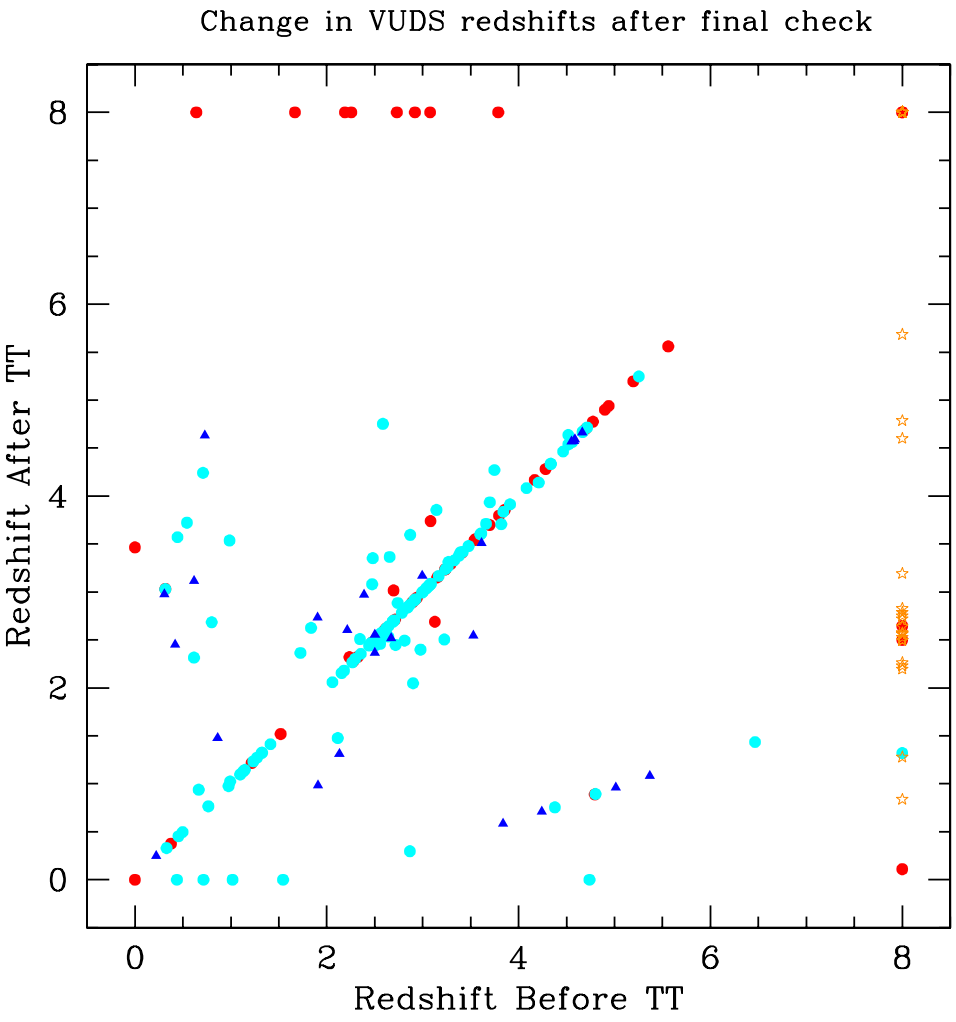

Fig. 4. Comparison between VUDS spectroscopic redshifts before and after the inspection of the tiger team (TT) of redshifts measured after a first measurement pass (see text). Only objects with a change are considered here. Represented in this figure are about 10% of all objects, including those with a redshift change (6%) or a flag change (4%). Red circles represent objects for which the reliability flag was downgraded after the inspection of the tiger team; filled cyan circles are objects with upgraded flags, blue triangles are objects retaining the same flag. Objects with undetermined redshifts (flag = 0) before the TT work are placed at $z_{\rm before} = 8$ and are represented with orange star symbols. Objects with undetermined redshifts after the TT work (either keeping their original undetermined status or those that the TT decided to downgrade) are the red circles at $z_{\rm after} = 8$.

photometric flux measurements agree excellently at better than the 5% level in all wavelengths $3650 \leq \lambda \leq 9350$ Å (Thomas et al. 2014). This is of particular importance when fitting the spectra to reference templates to derive internal galaxy properties (Thomas et al., in prep.). One of the last observations obtained on this program includes a number of repeated observations on a sub-sample of VUDS galaxies. When processed, it will allow estimating the redshift (velocity) measurement accuracy and to independently check the reliability of each of the redshift reliability flags (see below). Based on the previous VVDS, zCOSMOS, and VIPERS surveys with the same VIMOS instrument, we expect the redshift accuracy to be in the range $dz/(1+z) = 0.0005$–0.0007, or an absolute velocity accuracy 150–200 km s^{-1} (Le Fèvre et al. 2013b). Relative velocities in the same slit (along the slit profile) can be measured to a better precision using accurate spectral line fitting, for instance.

The 2D and 1D spectra are then available for spectroscopic redshift measurements using the EZ environment (Garilli et al. 2010). The core algorithm to find a redshift is the cross-correlation with templates, compared with a separate estimate of an emission line redshift when applicable. A key element for the cross-correlation engine to deliver a robust measurement is the availability of reference templates that cover a wide range of galaxy and star types and a wide range of rest wavelengths. This last point has to be carefully dealt with when measuring the highest redshift galaxies, as it is necessary that the templates extend far enough in the UV, bluer than the Lyman-912 Å limit, so that the wavelength overlap between the observed galaxy and the

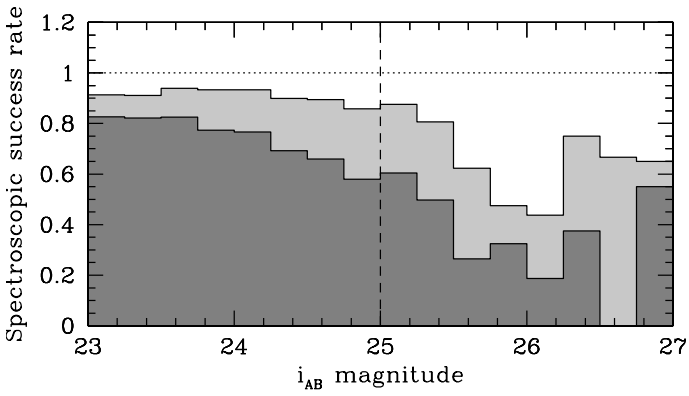

Fig. 5. Spectroscopic success rate versus $i_{\rm AB}$ magnitude for all objects with a redshift measurement (light grey) and all objects with a >75% reliable redshift measurement (flags 2, 3, 4, and 9; dark grey).

redshifted template is large enough to provide a robust correlation signal. We used templates built over the years from VIMOS observations for the VVDS (Le Fèvre et al. 2005b, 2013b) and the zCOSMOS survey (Lilly et al. 2007). As is relevant for $z > 2$, we have used templates with and without Lyman-α emission.

The redshift measurements were first obtained from an automated run with EZ. This served as a basis for a visual examination of each spectrum, with an iteration on the redshift measurement using EZ in manual mode, if necessary. All spectra were visually examined. For about half of the spectra, the

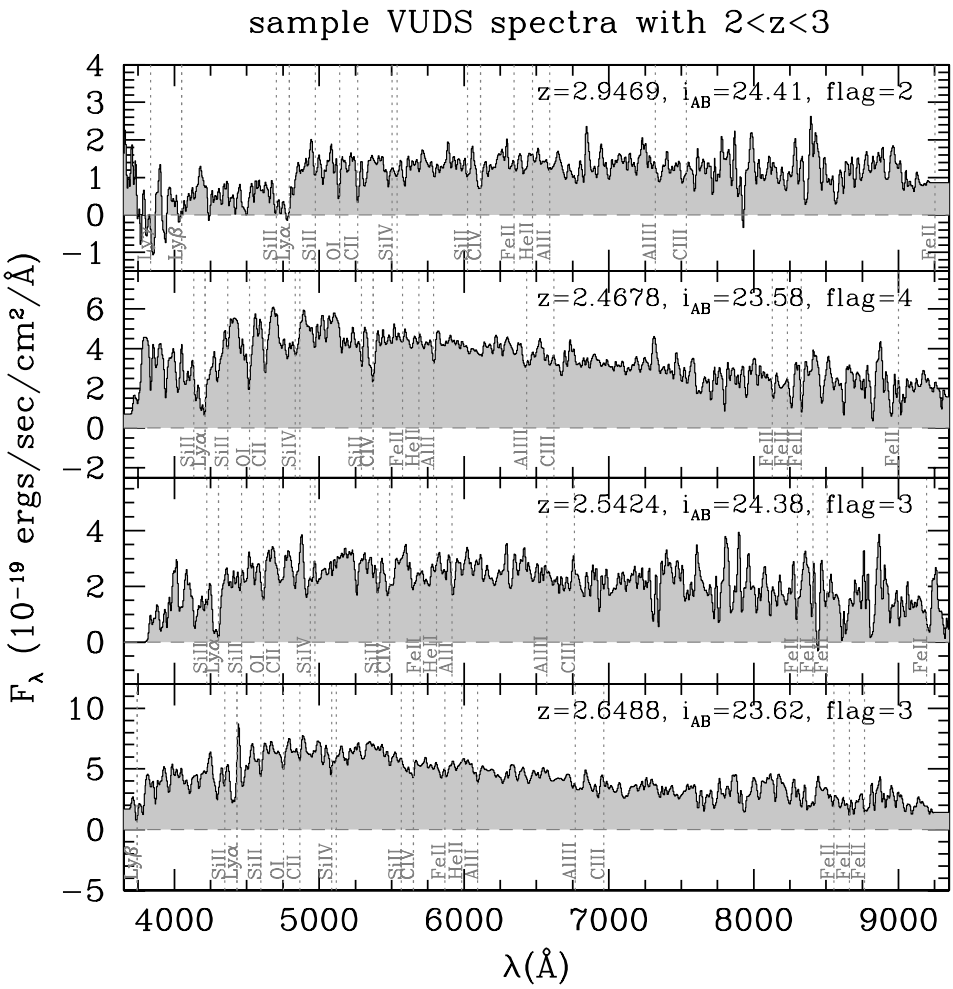

Fig. 6. Sample VUDS spectra in the range $2 < z < 3$. In this range Lyα just enters the VIMOS bandpass, and spectral features can be identified up to iron lines at ~2370 Å. Most of the population does not have Lyα emission.

redshift solution found from the automated EZ run was retained as the final one without further iteration, and the human intervention consisted only of assigning a reliability flag based on the identified spectral features. However, we found that at these high redshifts more than half of the spectra need manual intervention to properly measure a redshift. This is mainly due to residual defects in the spectra such as sky features residuals after sky subtraction or second-order spectra superimposition. The manual intervention consisted first of cleaning the spectrum from obvious noise residuals at the location of strong sky lines or zero-order projection. The EZ algorithm was then run again, and the main peaks of the correlation were examined within the graphical interface, which allowed overplotting the best template fit at each peak in the correlation signal. The best redshift was in general the second- or third-strongest correlation peak, or, in case of single line emission, the redshift was derived from a Gaussian fit of the line.

As the manual intervention remains an important feature in this process, we implemented a method to minimize measurement biases linked to one single person. One spectrum was measured by two team members separately, and these measurements were then compared to produce a single measurement agreed upon by the two measurers. With this scheme, we implemented the same redshift reliability estimator as developed for the CFRS (Le Fèvre et al. 1995) and refined for the VVDS (Le Fèvre et al. 2005b, 2013b), zCOSMOS (Lilly et al. 2007) or the VIPERS (Guzzo et al. 2014) surveys. The reliability of a redshift measurement is expressed with a flag giving the range of probability for a redshift to be correct. The reliability flag may take the following values:

- 0: No redshift could be assigned (the redshifts were then set to 9.9999).
- 1: 50–75% probability to be correct.
- 2: 75–85% probability to be correct.
- 3: 95–100% probability to be correct.
- 4: 100% probability to be correct.
- 9: spectrum with a single emission line. The redshift given is the most probable given the observed continuum, it has a ~80% probability to be correct.

The probabilities associated to these reliability flags are remarkably stable because the process involves several independent people, which smoothes out individual biases (Le Fèvre et al. 2013b).

VUDS enters a redshift domain that has never before been probed by spectroscopic redshift surveys on this scale. The expertise of the VUDS team members in measuring redshifts grew steadily as more and more of the data was being processed. Upon examination of the first measurements, we realised that redshifts were probably incorrectly assigned for a small but sizeable (~10%) fraction of the objects. Several standard cases for erroneous measurements were identified, including the possible confusion between early-M stars (M0–M3) and $z \sim 5$ absorption-line-only galaxies (going both ways), the assignment

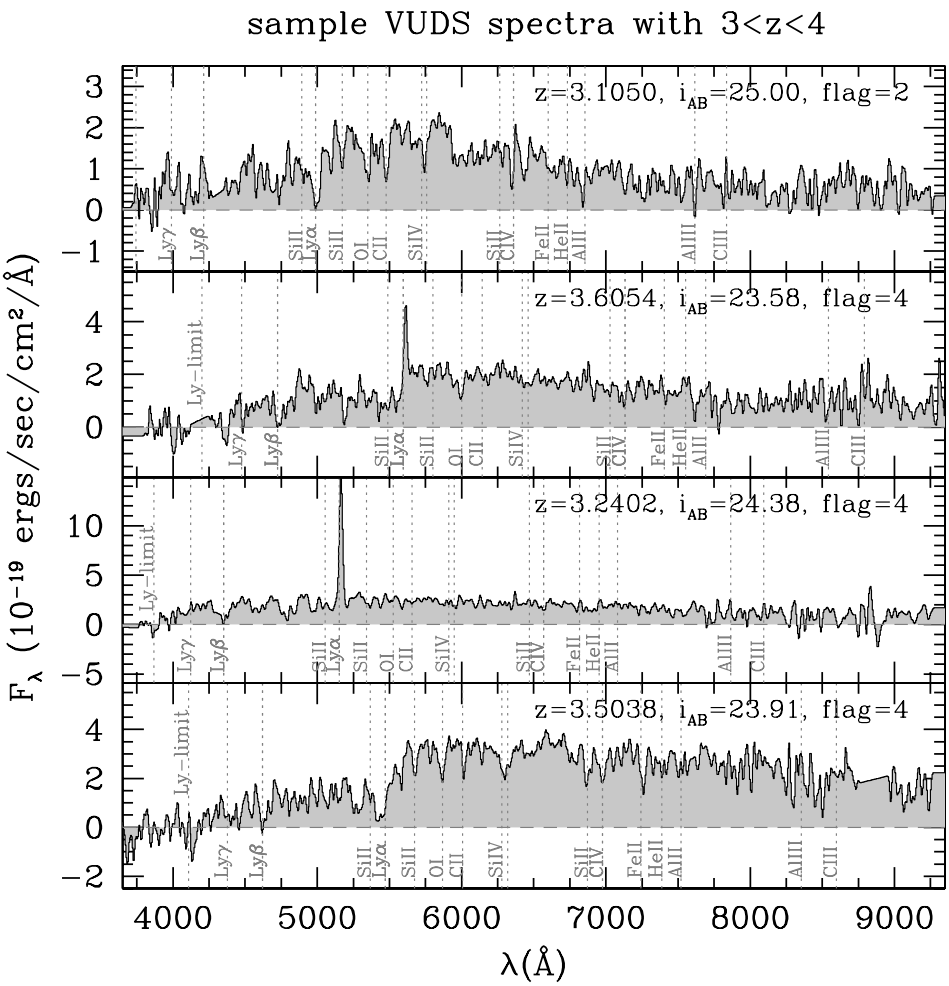

Fig. 7. Sample VUDS spectra in the range $3 < z < 4$. In the UV the Lyman limit at 912 Å enters the VIMOS bandpass at $z = 3$, and the VIMOS spectra are well sensitive to the IGM transmission. Farther in, the red spectral features can be identified up to CIII]. In this redshift range the fraction of Lyα emitters starts to rise, but the dominant population shows no Lyα emission.

Table 4. Main spectral features observed in VUDS spectra.

Spectral line	$\lambda_{\rm rest}$ (Å)	Line type
Lyman-limit	912.0	Continuum break
Lyman-γ	972.0	HI absorption
Lyman-β	1025.2	HI absorption
SiIIλ1192	1192.0	ISM, blend 1190+1193
Lyman-α	1215.7	HI emission & absorption
SiIIλ1260	1260.4	ISM
OI+SiII-1303	1303.2	ISM, blend
CIIλ1334	1334.5	ISM
SiIVλ1394	1393.8	ISM
SiIVλ1403	1402.8	ISM
SiIIλ1527	1526.7	ISM
CIVλ1549	1549.1	ISM, blend 1548.2+1550.8
FeIIλ1608	1608.5	ISM
HeIIλ1640	1640.0	Nebular
AlIIλ1671	1670.8	ISM
FeIIλ1855	1854.7	ISM
FeIIλ1863	1862.8	ISM
CIII]λ1909	1908.7	Nebular, blend 1907+1909
FeIIλ2344	2343.5	ISM
FeIIλ2371	2370.5	ISM
FeIIλ2402	2402.6	ISM
FeIIλ2594	2593.7	ISM
MgIIλ2796	2796	ISM

of Lyα-1215 Å instead of OII-3727 Å (or vice versa), and the setting of a continuum break to the Balmer-D4000 break rather than the Lyα break (or vice versa). In addition, the reliability flag as defined above was sometimes either too cautious when a measurer found a spectrum he/she was not yet familiar with, or too optimistic.

In view of this, we opted to create a "tiger team" (OLF, PC, EV, BG, DM, VLB, OLF, LP, LTa) charged with conducting an additional redshift check- This team was provided with a set of well-defined reference cases and their treatment. This redshift check was again made by two independent people who examined all the measured spectra, separately identifying which ones needed to have their redshift and/or reliability flag modified, and agreeing on the modifications. All pointings were examined by four pairs of two people, each pair proposing a list of modifications to be examined and agreed upon by the other "tiger team" members. We compare in Fig. 4 the old redshifts with the Tiger team redshifts, which summarizes this process. At the end of this process, about 10% of the objects had either a redshift or a flag change. While this does not guarantee that there are no more obvious "catastrophic failures" in spectroscopic redshift measurements, this process ensures a homogeneous treatment of all spectra and reduces the main degeneracies present in measuring the redshifts of high-redshift galaxies. Obviously, for the fainter objects where the information content of the spectra was insufficient to solve a possible degeneracy, the reliability flag was assigned to the "flag 1" category.

One key element of the selection function of the VUDS sample is the target sampling rate (TSR) defined as the ratio of the observed galaxies (all reliability flags) to the underlying parent

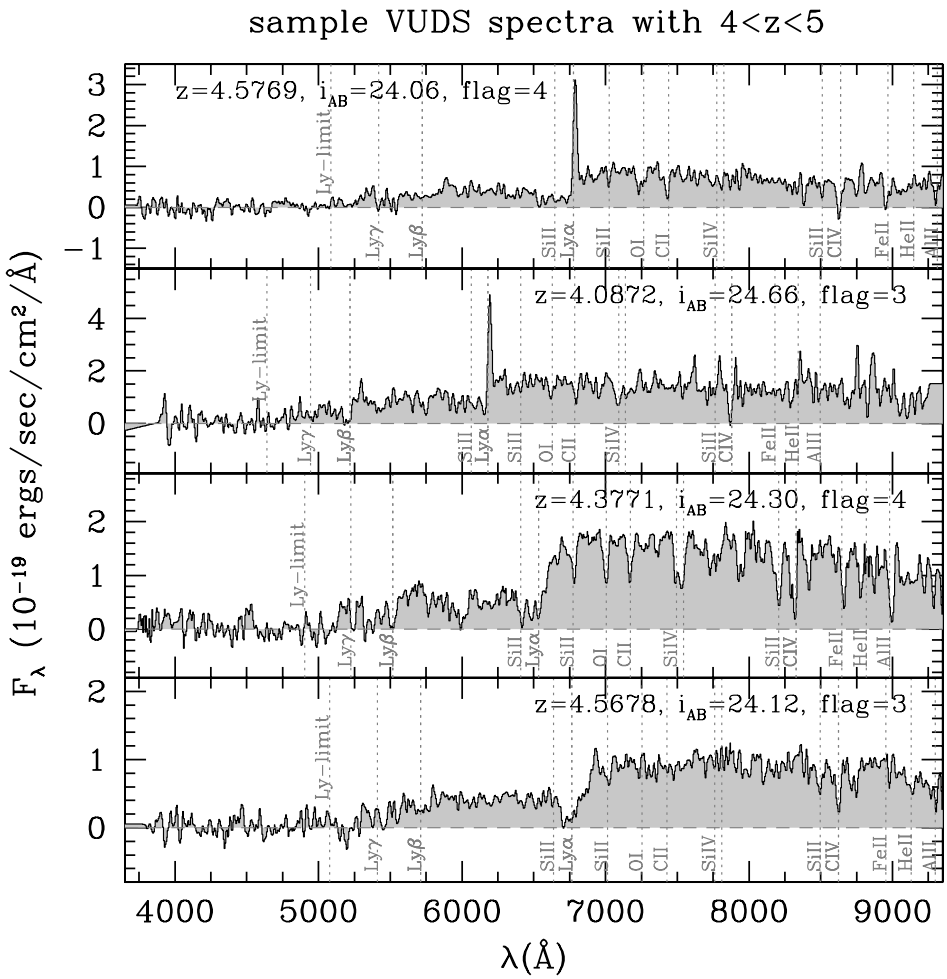

Fig. 8. Sample VUDS spectra in the range $4 < z < 5$. The observed UV rest-frame extends from below the Lyman limit up to CIV-1549 Å.

photometric populations from which the spectroscopic targets have been selected. We found a global TSR of ∼30% for the VUDS survey, similar for the three observed fields. With respect to the total population with $i_{AB} \leq 25$, the parent sample of galaxies satisfying the VUDS selection criteria represents 10%, and hence the observed VUDS sample represents 3.3% of all galaxies with $i_{AB} \leq 25$. The most reliable redshifts including flag 2, 3, 4, and 9 account for 70.2% of the sample, and we advocate the use of these objects for most science analysis, properly weighting galaxies if appropriate. Objects with flag 1 represent 21.4%, and 8.4% of the targeted sample could not be measured (flag 0). The spectroscopic success rate (SSR) as a function of magnitude is shown in Fig. 5. Down to $i_{AB} = 25$, 91% of the targets have a redshift measurement (flags 1, 2, 3, 4, 9), and 74.3% have a reliable measurement (flags 2, 3, 4, 9). This fraction is decreasing to 58% in the last 0.25 mag bin before $i_{AB} = 25$. The spectroscopic success rate then decreases with magnitude with a reliable redshift obtained for ≃30% of the galaxies targeted at $i_{AB} = 26$. A complete description of the survey selection function including the analysis of the spectroscopic success rate at different redshifts will be provided elsewhere (Tasca et al., in prep.).

The experience gained in this process is invaluable for future massive high-redshift surveys. As in Le Fèvre et al. (2013b), we emphasize that measuring the redshift at these high redshifts is a complex process that deserves dedicated and expert care beyond a simplistic "good" vs. "bad" redshift measurement scheme to fully exploit the information content of faint-object spectroscopy at the instrumental limit. This is further discussed in Sect. 3.5 in view of the a posteriori comparison between spectroscopic and photometric redshifts.

3.4. VUDS spectra

We present sample spectra over the redshift range of the survey in Figs. 6 to 9. The S/N per sampling element (∼7 Å) of the spectra at 1500 Å rest-wavelength has a mean of $S/N = 4.5$, and $\sigma_{S/N} = 2.1$, the S/N per spectral resolution element being ∼2× higher. This gives access to a range of spectral features and properties for each individual galaxy. The main spectral lines identified in individual spectra are Lyman-α 1215 Å (in emission or in absorption), OIλ1303, CIIλ1334, the SiIV–OIV doublet at λ1394–1403 Å, SiIIλ1527, CIVλ1549, FeIIλ1608, HeIIλ1640, AlIIλ1671, AlIIIλ1856, and CIII]λ1909 (see the list in Table 4). Below Lyman-α and depending on the IGM absorption, Lyman-β, Lyman-γ, and the Lyman limit at 912 Å can be identified. The average spectral properties in different redshift ranges are described in Sect. 4.3.

An overview of the spectra of the VUDS galaxy population over $2 < z <\sim 6$ is shown in Fig. 10. This figure is built from all spectra with reliability flags 3 and 4 in $2 < z < 4$ and all spectra with flags 2, 3 and 4 for $z > 4$ assembled in one single image, one spectrum per image line. The display is quite striking as the eye is able to follow up some of the weakest spectral features up to the highest redshifts. The Lyα line is readily visible in absorption or emission throughout the redshift range, with the blue wing of

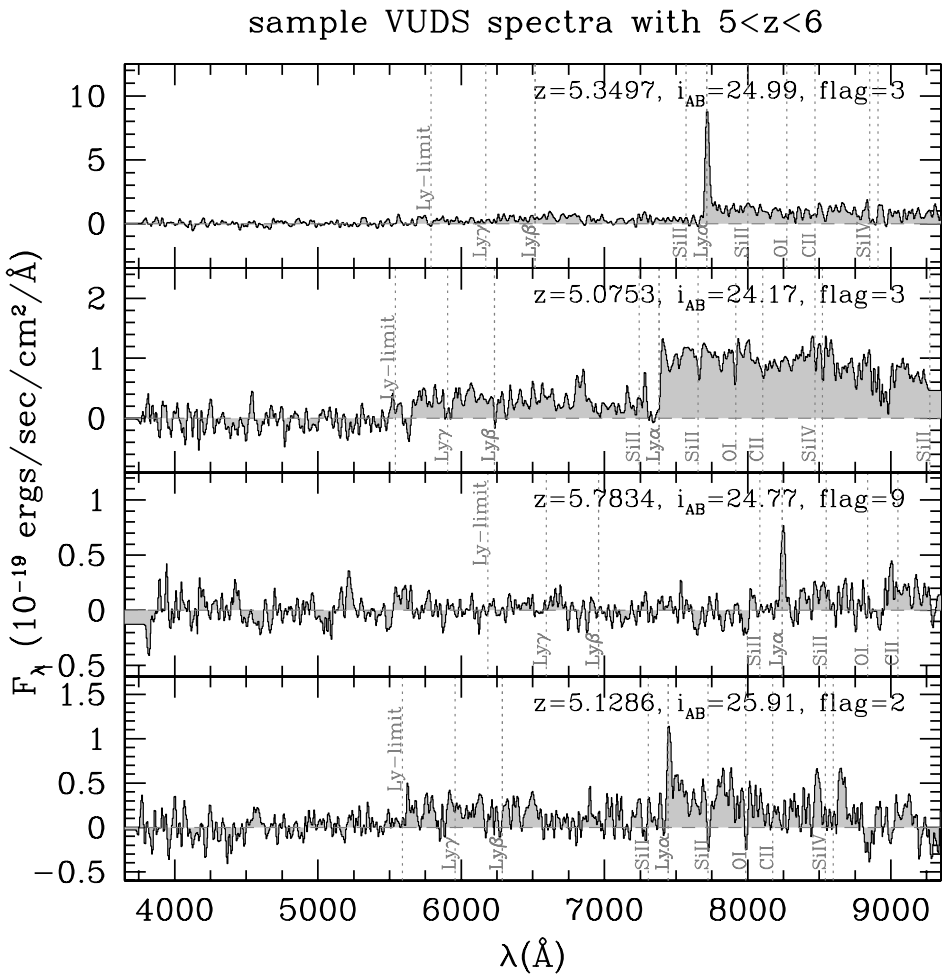

Fig. 9. Sample VUDS spectra in the range $5 < z < 6$. When the IGM transmission becomes high, the main spectral features used for the redshift determination are the spectral break produced by the IGM below Lyα and the Lyα line itself. The number of galaxies with Lyα in emission is about equivalent to galaxies with Lyα absorption (see Cassata et al. 2014, for a detailed discussion).

the broad damped Lyα clearly visible. At the higher redshifts, one can note the Lyβ, Lyγ, and Lyman-break (912 Å).

3.5. Comparison between spectroscopic and photometric redshifts

With VUDS targets selected in large part from their photometric redshifts (Table 2), we here compare the photometric redshifts $z_{\rm phot}$ computed from the multi-wavelength dataset and used as an input to the target selection, and the spectroscopic redshifts $z_{\rm spec}$. We compare $z_{\rm phot}$ and $z_{\rm spec}$ for the VUDS sample with reliable flags 3 and 4 in Fig. 11 (bottom left panel). Because close to 100% of the $z_{\rm spec}$ (flags 3, 4) represent the reality, we can directly test the accuracy and degeneracies of the $z_{\rm phot}$. We present in Fig. 12 the distribution of $\delta z = (z_{\rm spec} - z_{\rm phot})/(1 + z_{\rm spec})$ for flags 3+4 and 2+9 for $z < 1.5$ and $z > 2$ separations arbitrarily chosen to distinguish a low-redshift regime where the $z_{\rm phot}$ computation heavily relies on rest-frame visible-domain features like the D4000 spectral break, and a high-redshift domain where the computation rests on UV rest-frame features like the Lyα break produced by the intervening IGM and the Lyman-continuum limit. The width of the distribution for flags 3+4 below redshift $z = 1.5$ is an excellent $\sigma(\delta z/(1 + z)) = 0.02$, particularly in the COSMOS and ECDFS fields, which benefit from medium-band photometry. Above redshift $z = 2$, it is about twice as high, which is still excellent, but signals the increasing difficulty to assign accurate photometric redshifts from broad-band photometry alone.

It is immediately visible from comparing the photometric redshifts and spectroscopic redshifts for the best reliability flags (Fig. 11, bottom left panel) that there is a secondary tight relation with a low $z_{\rm phot}$ corresponding to a high $z_{\rm spec}$, which is easily explained by the degeneracy between the D4000 continuum break and the Lyman-α break when computing $z_{\rm phot}$ and our use of the secondary peak of the $z_{\rm phot}$ PDF to select spectroscopic targets. We draw in Fig. 11 the relation $z_{\rm phot} = (1215/4000)\times(1+z_{\rm spec})-1$ and ±15% around this mean. As seen in the bottom left panel, a number of galaxies are well within these limits, representing 9% of the flag 3 and 4 sample at $z > 2$. In all, 95.2% of our flag 3+4 sample at $z_{\rm spec} > 2$ satisfy either $z_{\rm spec} = z_{\rm phot}$ or $z_{\rm phot} = (1215/4000)\times(1+z_{\rm spec})-1$ within 15%, meaning that our selection function is particularly effective in picking up galaxies at these redshifts, with a low "catastrophic failure" rate, as further discussed in Tasca et al. (in prep.).

We can use the distribution of $(z_{\rm spec}, z_{\rm phot})$ for flags 3 and 4 to evaluate the level of agreement between $z_{\rm phot}$ and $z_{\rm spec}$ for other spectroscopic reliability flags 2, 1, and 9. The comparison between $z_{\rm phot}$ and $z_{\rm spec}$ for reliability flag 2, 1 and 9 is presented in Fig. 11. The distribution of galaxies for flags 1, 2, and 9 is qualitatively similar to the distribution for flags 3 and 4, with the 1:1 and the 4000:1215 relationships well populated. For flags 2 and 9 and $z > 2$ we find $\sigma(\delta z) = 0.044$, which is not much different from the flags 3 and 4 distribution, and with about 75% to 80% of the objects in this category within 15% of the 1:1 and 1215:4000 relations, which fully supports that these redshifts have a high level of reliability. As noted above, the secondary

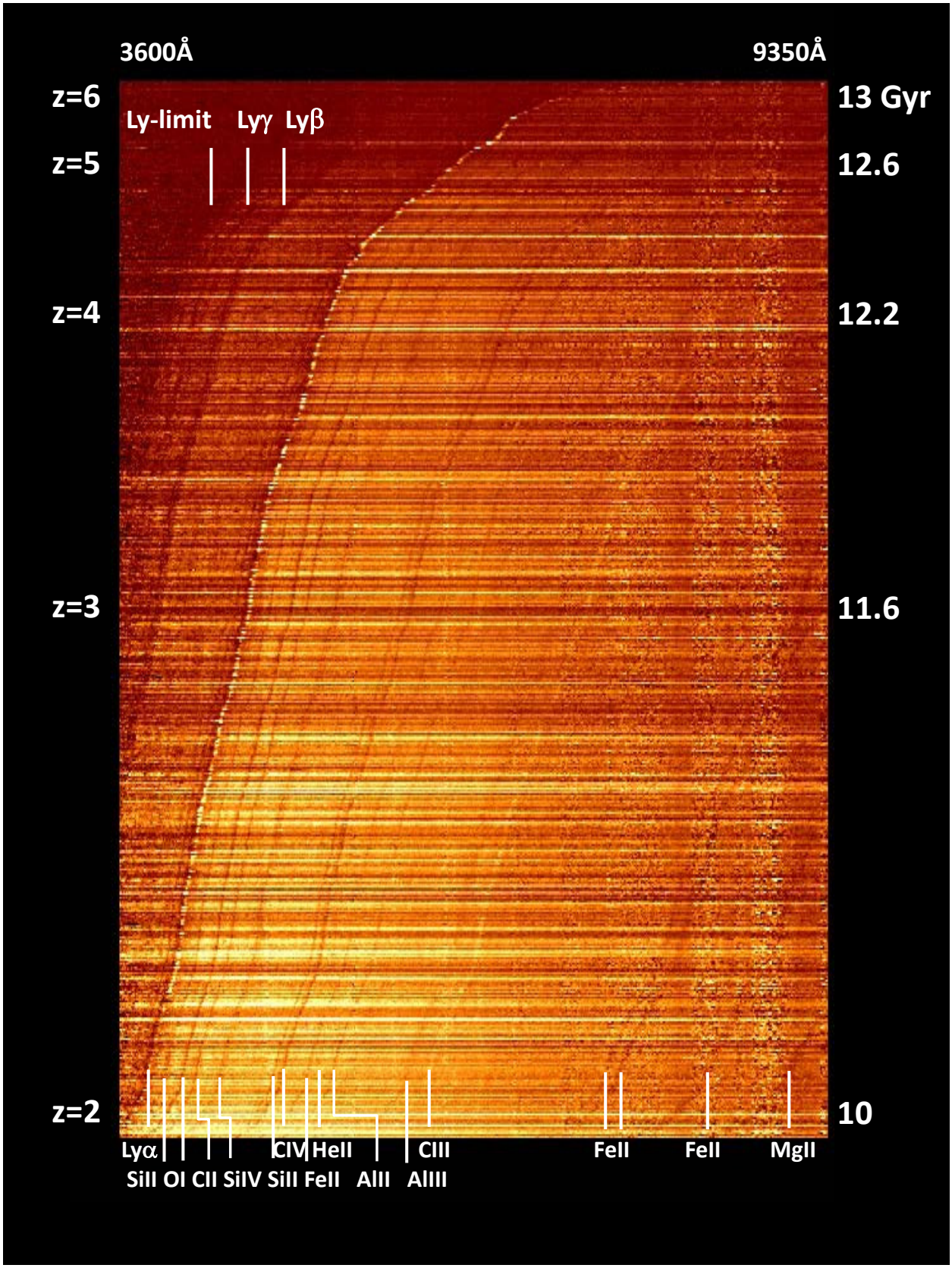

Fig. 10. Overview of the spectra obtained in the VUDS survey, with the wavelength extending from 3650 to 9350 Å on the *X*-axis. The redshift increases (in a non-linear way), as indicated along the left *Y*-axis, with the corresponding look-back time indicated along the right *Y*-axis. The image is build with the spectra of all $2 < z < 4$ VUDS galaxies with flags 3 and 4, and all spectra with flags 2, 3 and 4 for $z > 4$, ordered one per image line by increasing redshift. All the main emission and absorption lines can be readily identified in this image, even faint ones, thanks to the increased contrast produced by the continuous display of spectra. The main spectral lines are identified at the top left (below Lyα) and at the bottom of the plot (above Lyα), as listed in Table 4. The vertical bands appearing at fixed wavelength in the red correspond to increased residual noise after subtracting the strong atmospheric OH-bands.

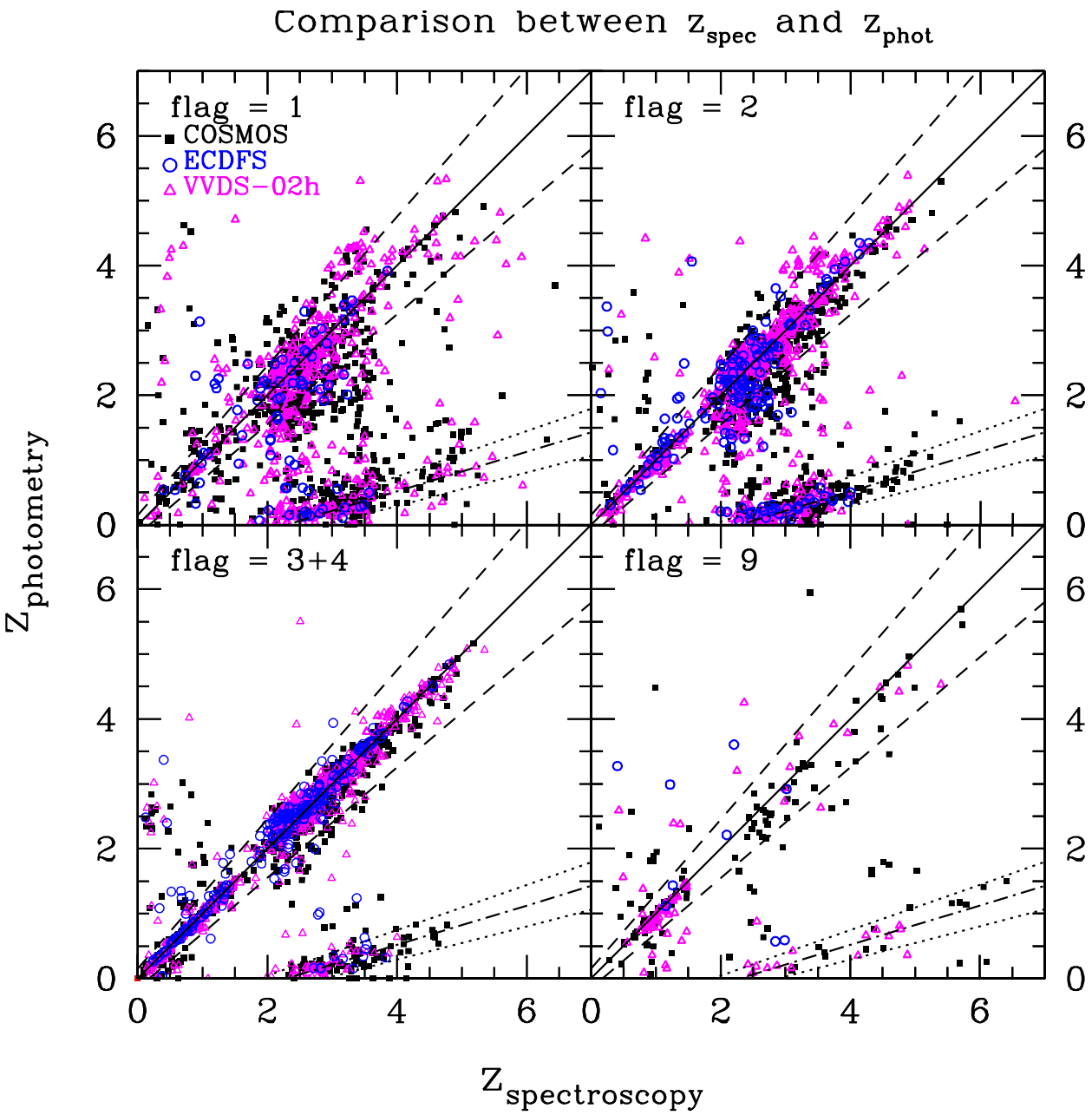

Fig. 11. A posteriori comparison between VUDS spectroscopic redshifts and the SED-derived photometric redshifts using the Le Phare code. *Top-left*: VUDS galaxies with spectroscopic flags 1 (≃50–70% reliable), *top right*: VUDS galaxies with spectroscopic flags 2 (≃75–85% reliable), *bottom left*: VUDS galaxies with spectroscopic flag 3 and 4 (95–100% reliable), *bottom-right*: VUDS galaxies with spectroscopic flags 9 (≃80% reliable). Galaxies in the three different fields are identified as filled squares (COSMOS field), open triangles (VVDS-02h), and open circles (ECDFS). The 1:1 equality relation is drawn as a continuous line, and 15% errors expressed as $0.15 \times (1 + z)$ are drawn as dashed lines. The known degeneracy of photometric redshifts between a Balmer-4000 Å break and a Lyα 1215 Å break is identified by the dotted-dashed line, with 15% errors drawn with dotted lines.

peak in these distributions for $z > 2$ is produced by the degeneracy betweeen the D4000 and 1215 Å continuum breaks. This peak is more pronounced for flags 2 and 9, with about 23% of the objects in this category within 15% of the 1215:4000 relation, meaning that the objects with these reliability flags are more prone to this degeneracy. A possible reason is that the magnitudes of flags 2 and 9 objects are on average fainter than the flag 3 and 4 counterparts. Defining the catastrophic failure rate in the selection of $z > 2.4$ VUDS galaxies as the fraction of galaxies that are outside either $|z_{\rm spec} - z_{\rm phot}| \leq 0.15 \times (1 + z_{\rm spec})$ or $z_{\rm phot} - (1215/4000) \times (1 + z_{\rm spec}) - 1 \leq 0.15$, it is 20% for flag 2, 37% for flag 1, and 24% for flag 9. Taking into account the intrinsic catastrophic failure rate of 5% for photometric redshifts as observed for flags 3 and 4, this gives a qualitative estimate on the reliability level of the different spectroscopy flags.

Based on the excellent match between spectroscopic and photometric redshifts obtained for flag 3 and 4, we added a decimal point to the reliability flag as defined in Sect. 3.3, which translates the level of agreement between the spectroscopic redshift and the photometric redshift for each galaxy. This decimal point may take five different values from 1 for a poor agreement to 5 for an excellent agreement; more specifically: *.1 means that

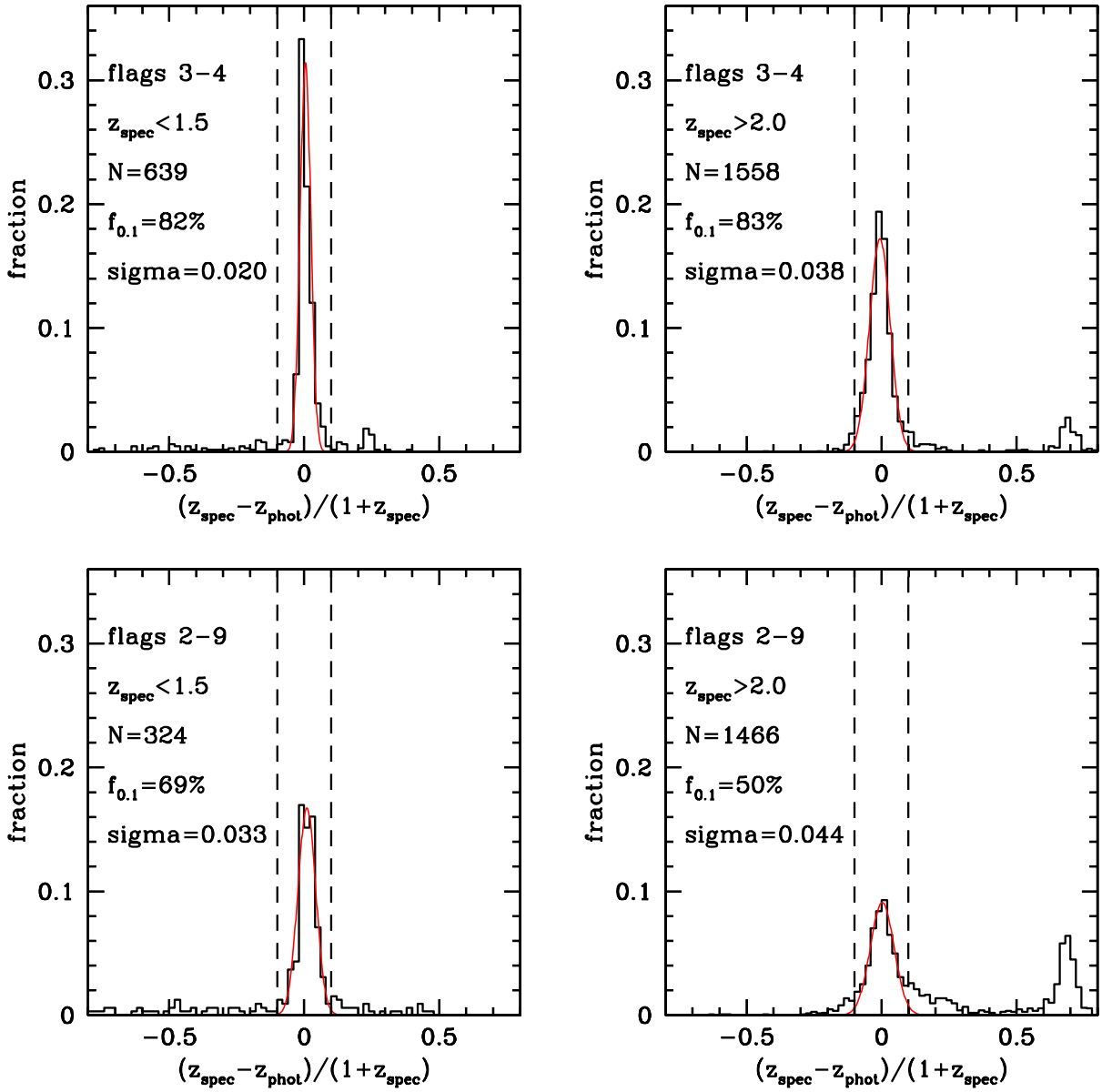

Fig. 12. Distribution of the difference between photometric redshifts and VUDS spectroscopic redshifts for flags 3 and 4 (*top panels*) and flags 2 and 9 (*bottom panels*) for redshifts $z < 1.5$ (*left panels*) and redshifts $z > 2$ (*right panels*). The number of galaxies is indicated in each panel together with the σ of the distribution and the fraction of galaxies satisfying $\delta z = (z_{\rm spec} - z_{\rm phot})/(1 + z_{\rm spec}) \leq 0.1$. The distribution peaked at 0 is for the main sample, while a secondary peak appearing beyond $\delta z = 0.5$ is produced by the degeneracy between the D4000 and the 1215 Å continuum breaks (see text).

the spectroscopic and photometric redshifts have a difference $dz = | z_{\rm spec} - z_{\rm phot} | /(1 + z_{\rm spec}) \geq 0.5$, *.2 is for $0.3 \leq dz < 0.5$, *.3 for $0.2 \leq dz < 0.3$, *.4 for $0.1 \leq dz < 0.2$, and *.5 for $dz < 0.1$. Adding a *.5 decimal therefore further increases the reliability of the spectroscopic redshift measurement, while a *.1 decimal would lower it instead. However, for the higher spectroscopic reliability flags 3 and 4, a low photometric decimal *.1 or .2 would instead indicate that the photometric redshift is probably incorrect. This scheme allows defining a sample that depends on the reliability level required by a particular analysis.

This analysis brings two general comments for studies based on photometric redshifts. First, if VUDS targets had been selected only based on the primary peak of the $z_{\rm phot}$ PDF, ~17.5% of the sample with $z \geq 2$ would have been lost compared to our selection. Second, for studies only based on a $z_{\rm phot}$ sample, which necessarily assign a redshift using the primary peak of the redshift PDF, 14.2% of the high-redshift galaxies would be missed because they would be incorrectly placed at low redshift instead of $z > 2.3$. This average value shows a variation with redshift, which will be discussed in a forthcoming paper.

4. General properties of the VUDS sample

In this section we report on the main properties of the VUDS sample, giving an overview of the parameter space probed by the survey. At the time of writing, the VUDS sample contains 6250 objects with a measured redshift, including 6003 galaxies, 20 AGNs, and 227 stars, while no redshift measurement could be obtained for 750 objects. These numbers will increase by 15–20% when data processing is completed. The projected

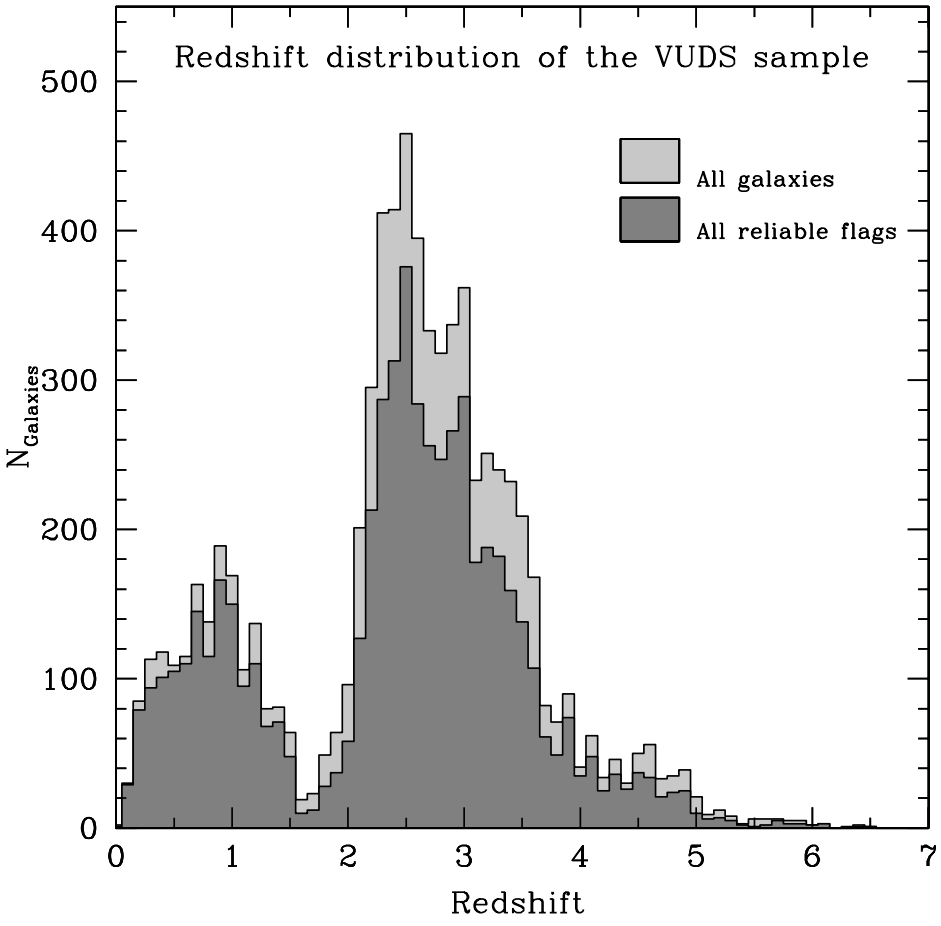

Fig. 13. Current redshift distribution from 7825 galaxies already processed in the VUDS survey for all objects with a redshift measurement (light grey) and all objects with a >80% reliable redshift measurement (flags 2, 3, 4, and 9; dark grey).

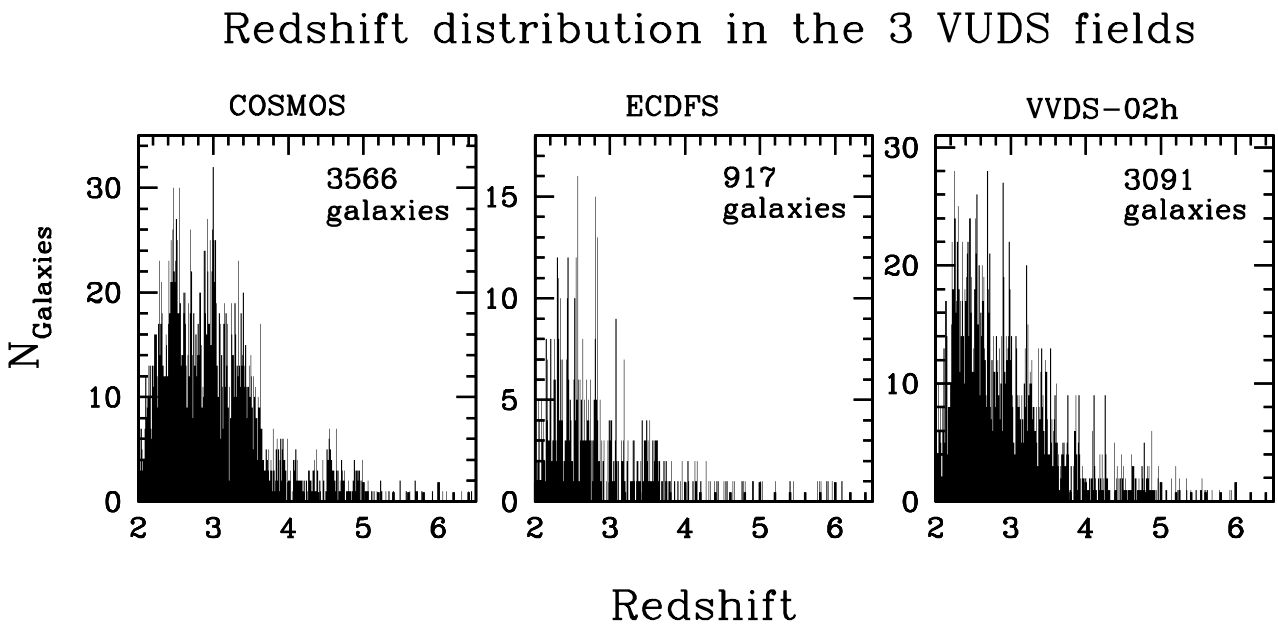

Fig. 14. Distribution of redshifts measured by VUDS in the 3 fields: 3566 galaxies in COSMOS, 917 in ECDFS, and 3091 in VVDS-02h (all objects with a redshift measurement are used).

sky distribution of the VUDS sample follows the layout of the VIMOS pointings as identified in Figs. 1 to 3. With eight pointings on the COSMOS field, ~4150 objects previously without measurements have been observed and ~3700 have now spectroscopic redshift measurements (these numbers are being revised following the last data processing), covering a total area of 1800 arcmin^2. Over 1125 arcmin^2 in the VVDS-02h field the data for ~2300 targets have been processed and ~2100 objects have now spectroscopic redshifts, and we expect 20% more when data processing is completed. In the ECDFS, one pointing

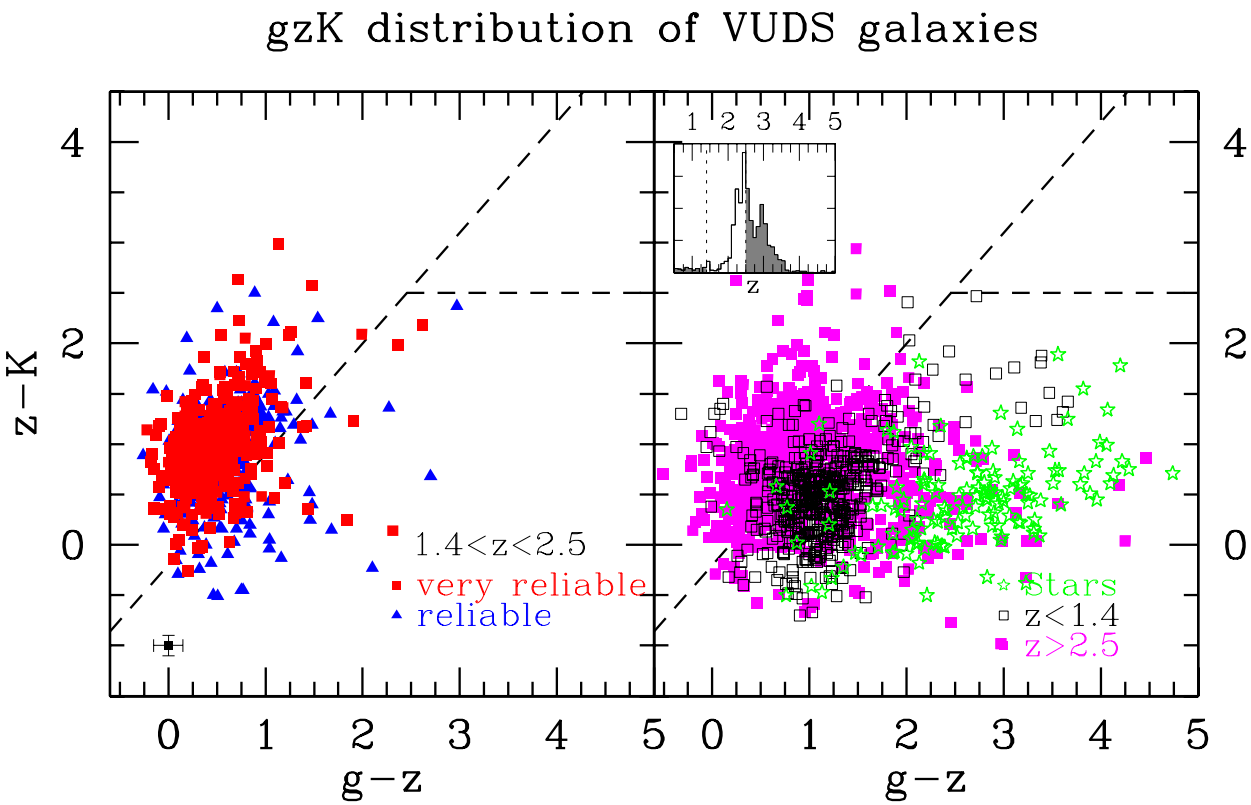

Fig. 15. *Left panel*: $(g - z)$ vs. $(z - K)$ colour–colour diagram for VUDS galaxies with $1.4 < z < 2.5$ (flags 3 and 4: red squares, flag 2: blue triangles). The average colour errors are indicated in the lower left corner. Galaxies in this plot are detected in all three bands at more than 3σ (95% of the sample). The *gzK* selection would have selected 91% of the VUDS galaxies with $1.4 < z < 2.5$. *Right panel*: same for galaxies either with $z < 1.4$ (open squares) or $z > 2.5$ (magenta filled squares). Stars are represented by green star symbols. There is a high level of contamination as 58% of galaxies in the selection area of the *gzK* are outside the redshift range $1.4 < z < 2.5$, coming mostly from galaxies at $z > 2.5$. (*inset*) redshift distribution of galaxies in the *gzK* selection area, the grey shaded histogram represents galaxies outside the redshift range $1.4 < z < 2.5$.

has been processed so far with ~550 objects observed and ~500 with a redshift measurement, and with two more pointings to process (one with LR and one with MR grisms), we expect this number to increase by about 60%. We use the current sample to discuss below the general properties of the sample.

4.1. Sample properties

The efficiency of the survey target selection can be estimated from the redshift distribution of the observed sources.

The redshift distribution of the VUDS sample is shown in Fig. 13. The $N(z)$ is bimodal, with a high-redshift component from $z \sim 2$ to $z \sim 6.5$ and a lo- redshift component mainly at $z < 1.5$. The sample above $z = 2$ is the sample of interest for the main science goals of VUDS; it represents about 80% of the total sample, with currently more than 4500 objects with a redshift measured with $z \geq 2$, and, extrapolating for the remaining data to be processed the VUDS sample, it will contain ~6000 objects with $2 < z < 6.5$ in the end. VUDS is today the largest sample of galaxies with spectroscopic redshifts in any of the redshift bins $2 < z < 3$, $3 < z < 4$, $4 < z < 4.7$ or $4.7 < z < 5.3$, as further discussed in Sect. 5.

The sample below $z \simeq 2$ is made of several sub-samples: (i) galaxies for which the second peak of the $z_{\rm phot}$ PDF is at $z > 2.4$, but which were found to be at the lower redshift indicated by the first peak; (ii) galaxies for which the selection criteria for high redshift failed and that are instead located at low redshifts; (iii) galaxies with $i_{\rm AB} \leq 25$ that have been used as mask fillers and for which the $N(z)$ is expected to peak at $z \sim 1.5$ (Le Fèvre et al. 2013a); and (iv) some serendipitous sources falling in the slits by chance. The mean redshift for the sample above $z = 2$ is $\bar{z} = 3.0$. About 10% of the sample is above $z = 4$, and the high-redshift tail extends beyond redshift $z = 6$, the highest reliable redshift so far being $z = 6.5363$. The current redshift distribution for $z \geq 2$ in the COSMOS, ECDFS, and VVDS-02h fields is shown in Fig. 14. The redshift bin of $dz = 0.01$ enables showing the strong clustering present at all redshifts probed by the survey. Some of the densest peaks are remarkable examples of clustering in the early Universe, as discussed in Cucciati et al. (2014) and Lemaux et al. (2014a).

As our sample is $z_{\rm phot}$ selected, it is interesting to determine where the VUDS galaxies are distributed in several standard colour–colour diagrams. Following other studies (Kurk et al. 2013; Le Fèvre et al. 2013a), this a posteriori analysis gives the studies that use colour–colour selection an indication of both the efficiency of the selection and the contamination by galaxies at other redshifts than the redshift of interest in the selected colour space. We examine here the *gzK* diagram used to select galaxies with $1.4 < z < 2.5$, and the *ugr* diagram for galaxies with $2.5 < z < 3.5$. Other colour–colour diagrams like the *gri* or *riz* for $3.5 < z < 4.5$ and $4.5 < z < 5.5$ will be investigated in a forthcoming paper.

The BzK selection is based on the identification of the Balmer and D4000 break crossing the z band for $1.4 < z < 2.5$ (Daddi et al. 2004). We present the *gzK* diagram in Fig. 15, with the colour–colour area adjusted to take into account the

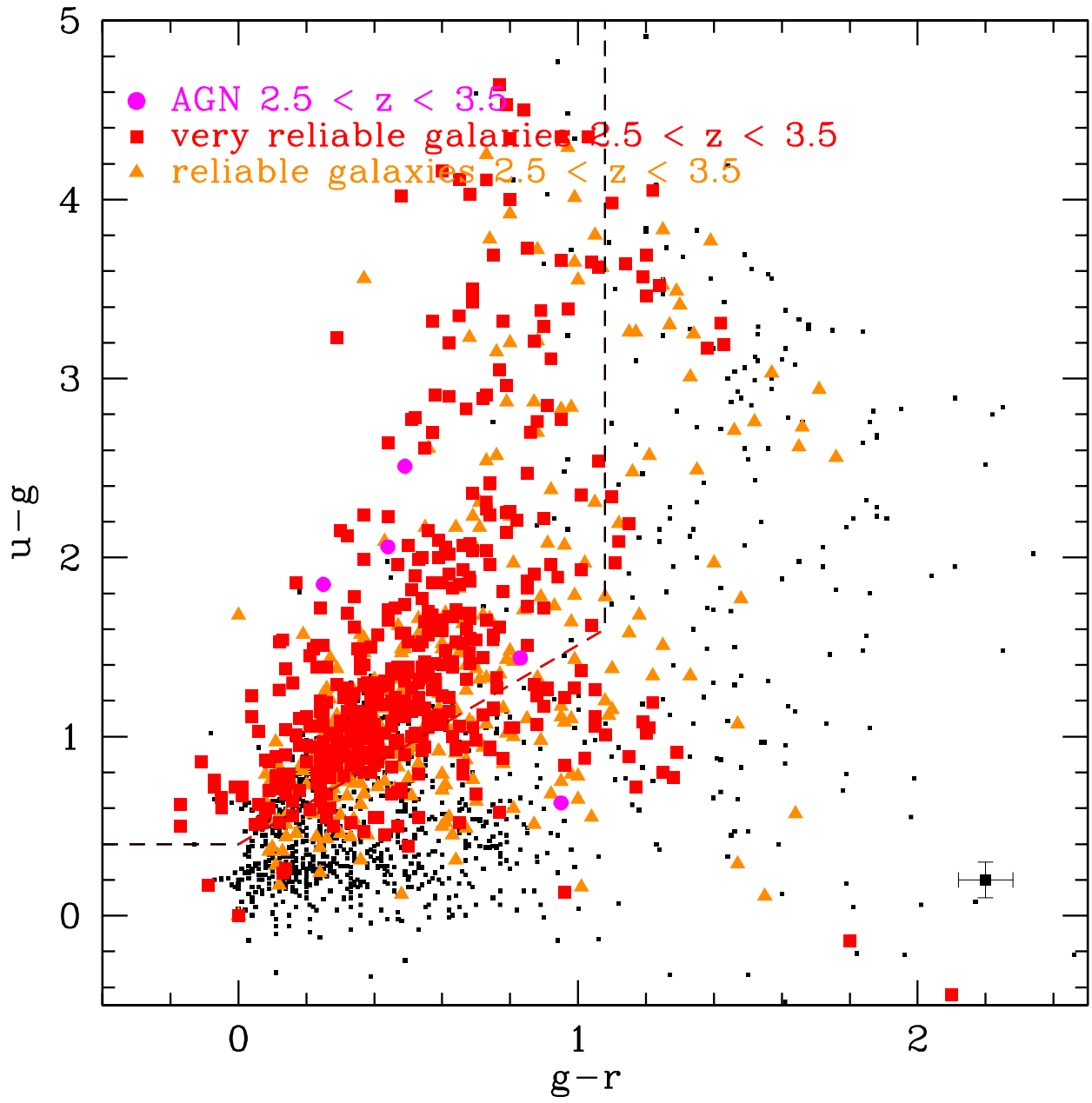

Fig. 16. $(u-g)$ vs. $(g-r)$ colour–colour diagram for VUDS galaxies with $2.5 < z < 3.5$. Galaxies with flags 3 and 4 are represented by red squares, galaxies with flag 2 by orange triangles while type I AGN are represented by filled magenta circles. The *ugr* selection would have selected 80% of the VUDS galaxies with $2.5 < z < 3.5$, but with a high level of contamination because 40% of galaxies in the selection area of the *ugr* are outside the redshift range $2.5 < z < 3.5$.

different wavelength coverage of the g filter compared to the B filter (Bielby et al. 2012; Le Fèvre et al. 2013a). The *gzK* criteria are efficient to select 92% of the VUDS galaxies with $K \leq 24$. However, we note that the level of contamination of a *gzK* selected sample down to $K_{\rm AB} = 24$ would be quite high as 58% of galaxies in the selection area of the *gzK* diagram selecting the $1.4 < z < 2.5$ redshift range would be outside this range at $z < 1.4$ or $z > 2.5$ (right panel of Fig. 15); at $K_{\rm AB} = 22$ we find this contamination to be lower, at the ~30% level. This trend is similar to that found by Le Fèvre et al. (2013a), who identified a magnitude-dependent contamination level. As the VUDS data are selected with $z_{\rm phot} > 2.4$, the contamination level is further enhanced compared to the pure i-band magnitude selection of the VVDS.

At higher redshifts, we show the distribution of VUDS galaxies with $2.5 < z < 3.5$ in the *ugr* colour–colour diagram in Fig. 16. Here again a large fraction ~80% of galaxies appear in the expected locus of the colour–colour diagram. The contamination by galaxies at $z < 2.5$ or $z > 3.5$ is quite high at about 40%. We note that we did not attempt to optimize the redshift range on the basis of the exact shape of the photometric bands used for the CFHTLS photometry used in this plot, but we rather elected to show the distribution of a large population.

This a posteriori colour–colour analysis shows that the VUDS sample is behaving as generally expected for galaxies at these redshifts. The photometric redshift selection allows identifying galaxies beyond the classical colour–colour locus of the *gzK* and *ugr* diagrams. We also point out the strong

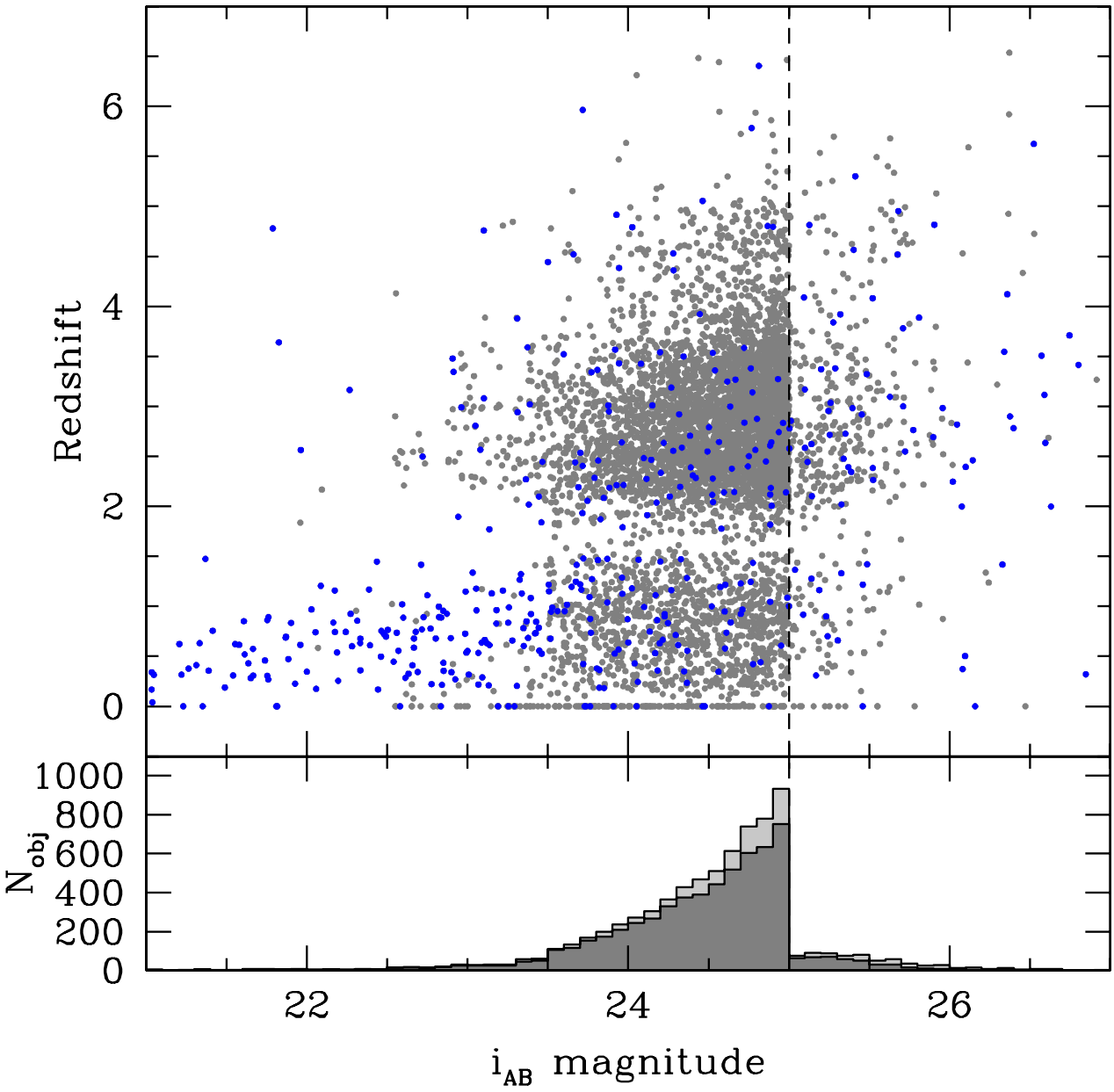

Fig. 17. *Top panel*: i_{AB} magnitude – redshift distribution for the full VUDS sample (grey points) and for serendipitous objects in the slits (blue points). *Bottom panel*: distribution of i_{AB} magnitudes in the VUDS survey for all objects observed (light grey), and for those with a redshift measurement (any non-zero flag, dark grey). The $i_{AB} = 25$ imposed on the sample selected by photometric redshifts is indicated. The fainter objects are pre-selected from one of the other colour or SED criteria.

contamination present in colour–colour selected samples from galaxies at other redshifts outside the targeted redshift range.

4.2. Absolute magnitudes, stellar masses, and star formation rates

The distribution of apparent magnitudes with redshift is shown in Fig. 17. In all, about 90% of the distribution is within $23 \leq i_{AB} \leq 25$, while about 10% have $25 \leq i_{AB} \leq 27$.

The VUDS sample covers a wide range of galaxy physical properties. Using the VUDS spectroscopic redshifts, we performed SED fitting of the multi-wavelength photometry using the code Le Phare (Ilbert et al. 2006), as described in Ilbert et al. (2013). We summarize here a few key points, but we refer to the recent description of the fitting process in Ilbert et al. (2013) for a detailed account and associated limitations. Galaxy luminosities are transformed into stellar mass using the best-fit synthetic template from a list of templates built from the stellar population synthesis models of Bruzual & Charlot (2003) with three metallicities ($Z = 0.004$, $Z = 0.008$, and solar $Z = 0.02$), and exponentially declining and delayed star formation rate with nine different τ values from 0.1 to 30 Gyr. We used the extinction law of Calzetti et al. (2000), and emission lines were added to the synthetic spectra as described in Ilbert et al. (2009). The output of this fitting process includes among other parameters the absolute magnitudes integrated into standard bands, stellar masses, star formation rates, and extinction. The distributions in

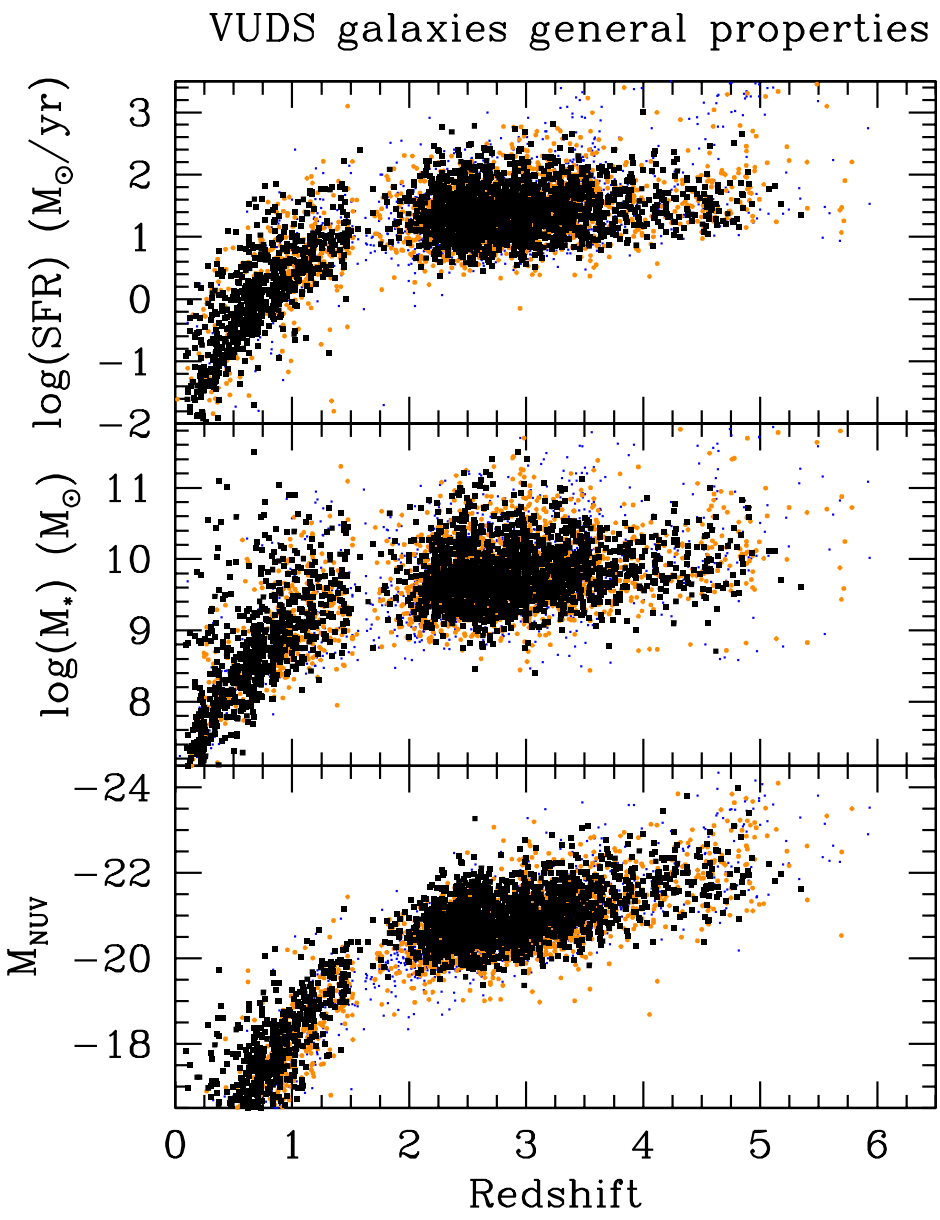

Fig. 18. Distribution of absolute u-band magnitudes (*bottom*), stellar masses (*centre*), and star formation rate (*top*). Stellar masses and star formation rates are derived from template SED fitting at the spectroscopic redshift (see text). Black squares are for galaxies with reliability flags 3 and 4, orange filled circles are for flag 2, and blue dots are for flag 1.

absolute near-UV (NUV; 2300 Å rest) magnitude, stellar masses, and star formation rate of the sample are presented in Fig. 18. At redshifts $z \sim 3$–4, the NUV absolute magnitude ranges from NUV = −20.5 to NUV = −23, the stellar mass from 10^9 $M_\odot$ to 10^{11} $M_\odot$, and the star formation rate from below 1 $M_\odot$/yr up to several hundred $M_\odot$/yr.

The VUDS survey therefore covers a large parameter space both in the observed properties and the physical properties of the sample galaxies.

4.3. Average spectral properties: stacked spectra

Stacked spectra were produced from previous surveys, for example, from Shapley et al. (2003) for $z \sim 3$, or for B, V and R dropout galaxies Vanzella et al. (2009). The large statistics and wavelength coverage of VUDS offers the opportunity of producing composite spectra over a wide redshift coverage. The average spectral properties of galaxies over the redshift range $2 \leq z_{\rm spec} \leq 6.5$ were derived from stacking VUDS spectra in different redshift bins. For each redshift bin, the average spectra were produced using the `odcombine` task in IRAF, averaging spectra after scaling to the same median continuum value, that is, luminosity weighted, and weighting spectra to their mean flux in the same rest-frame wavelength range. Average spectra using sigma clipping, removing at each wavelength data with a value 1.5–3 times the 1σ value, were compared to the straight weighted average described above, and very little difference was observed when there were many spectra (>50). For smaller samples, sigma clipping helps to improve the S/N of the stacks by removing the left-over signatures of the sky subtraction process, for example.

The average spectra of all galaxies for several redshift bins are shown in Figs. 19 to 23, together with the average spectra of those with and without Ly-α emission. We discuss some of the key features below.

We find that the fraction of galaxies with any trace of Lyα emission strongly changes with redshift with $30.6 \pm 1.8\%$ in $2 \leq z \leq 3$, $38.3 \pm 2.9\%$ in $3 \leq z \leq 4$, $61.6 \pm 7.0\%$ in $4 \leq z \leq 4.7$, and $66.6 \pm 14.2\%$ in $4.7 \leq z \leq 5.3$. The detailed properties of the

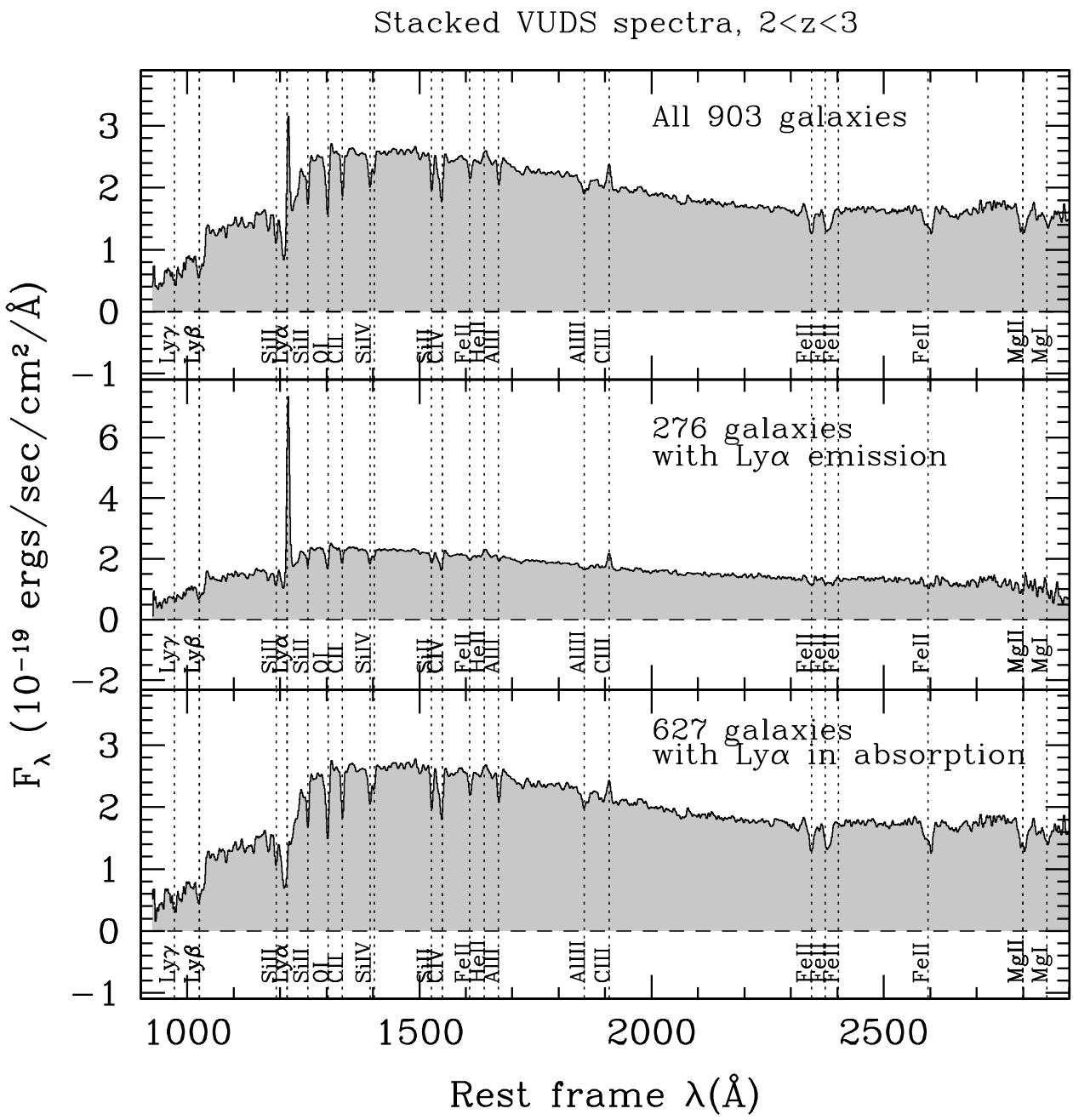

Fig. 19. Average rest-frame spectra (F_λ) of galaxies with flags 3 and 4 in VUDS with $2 \leq z \leq 3$: *top*: stack of all galaxy spectra; *middle*: stack of galaxies with Ly-α in emission; *bottom*: stack of galaxies with Ly-α in absorption (this stack is from a subset of the final sample available at the time of writing).

Lyα emitting fraction and implications are examined in detail in Cassata et al. (2015).

In addition to Lyα, several spectral features are noteworthy, as indicated in Table 4. The main absorption features redder than Lyα include the SiIIλ1260, OIλ1303, CIIλ1334, SiIVλ1394/1403, SiIIλ1527, and CIVλ1549 lines. In emission, weak CIII]λ1909 is quite common, and S-shape absorption-emission features can be identified for SiIIλ1260, OIλ1303 or CIVλ1549, for example, which is indicative of strong outflows. The HeIIλ1640 emission is ubiquitous, as seen on all spectra where this line is in the wavelength range (Figs. 19 to 21). This line, when several hundreds of km s^{-1} in width, indicates the presence of strong winds around Wolf-Rayet stars. If narrow, it may indicate some other processes, such as a population of low-metallicity stars with properties similar to Population III (Cassata et al. 2013).

Below the Lyα line, the main features identified in galaxies at these redshifts are SiIIλ1192 and then the Lyβ and Lyγ lines, followed by the Lyman-limit, which produces a continuum break at 912 Å. It is interesting to note that the flux below 912 Å in our stacked spectra is not zero, as would be expected if the Lyman-continuum escape fraction was 0%. We observe a significant detection of flux below the Lyman-limit in the stacked spectra of galaxies at $3 < z < 4$, $4 < z < 4.7$ and $4.7 < z < 5.3$. The ratio of continuum flux density in the [1400, 1500] Å range over

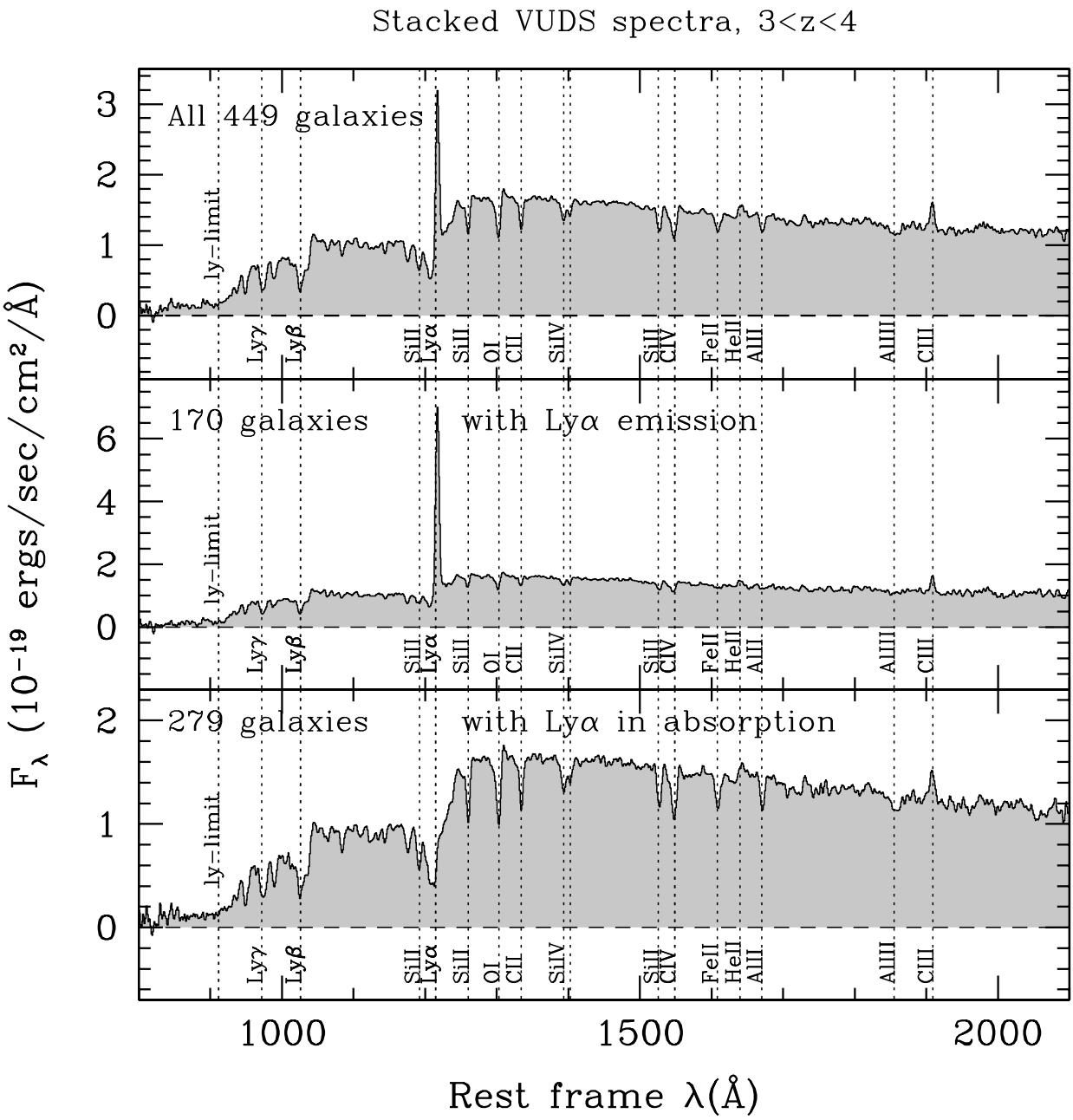

Fig. 20. Average rest-frame spectra (F_λ) of galaxies with flags 3 and 4 in VUDS with $3 \leq z \leq 4$: *top*: stack of all galaxy spectra; *middle*: stack of galaxies with Ly-α in emission; *bottom*: stack of galaxies with Ly-α in absorption (this stack is from a subset of the final sample available at the time of writing).

the flux in [800, 900] Å range below the 912 Å Lyman-limit is $f_{1500}/f_{900} = 32 \pm 3$, 39 ± 5, and 33 ± 10, respectively, in these three redshift bins. Although these measurements are based on a much larger sample that covers a wider redshift range, these values are similar to the observed value of 58 ± 18 reported by Shapley et al. (2006) at $z \sim 3$. While it is tempting to interpret this in terms of the Lyman-continuum escape fraction, we note that at the faint magnitudes we are observing, the flux observed below 912 Å in stacked spectra might also be coming in part from objects contaminated by lower redshift interlopers that produce observed flux below that of the Lyman-limit at the rest-frame of the distant source (Vanzella et al. 2010). The *observed* non-zero flux below 912 Å has consequences on the selection of high-redshift galaxies based on the Lyman-break technique, as the expected colours of high-redshift galaxies are affected by a priori hypotheses, for instance on the f_{1500}/f_{900} ratio (Cooke et al. 2014). This and the corrected Lyman escape fraction will be analysed in forthcoming papers.

Our stacked spectra beautifully show the evolution of the "staircase" pattern of IGM absorption as a function of redshift produced by continuum blanketing from the Lyman series of galaxies along the line of sight in the probed volume (Madau 1995). The comparison of the observed mean and distribution of IGM absorption properties as a function of redshift in VUDS to the models of Madau (1995) and Meiksin (2006) is extensively discussed in Thomas et al. (2014).

A detailed analysis of the spectral properties of stacked spectra and individual galaxies in the VUDS sample will be presented in forthcoming papers.

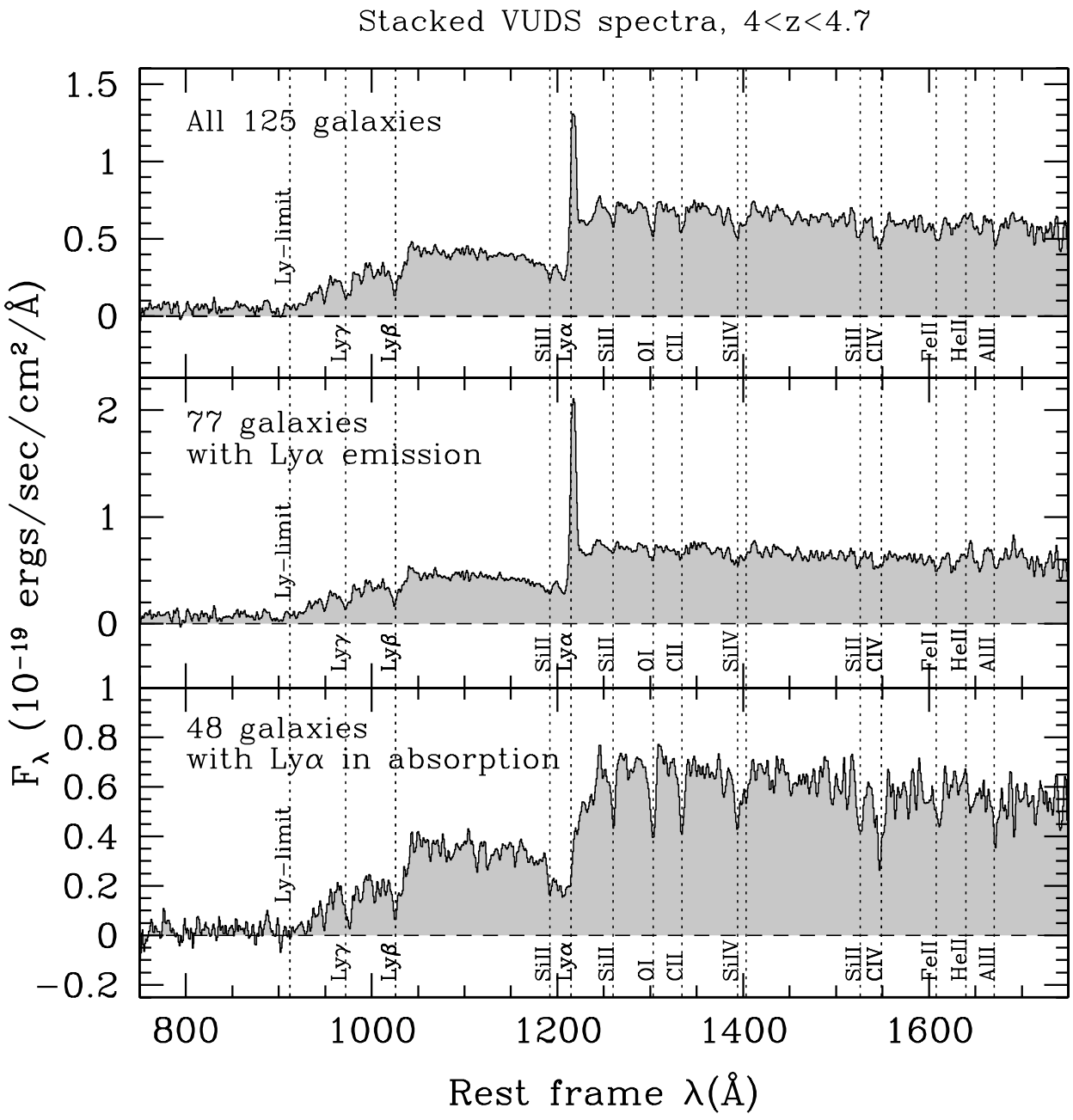

Fig. 21. Average rest-frame spectra (F_λ) of galaxies with flags 2, 3 and 4 in VUDS with $4 \leq z \leq 4.7$: *top*: stack of all galaxy spectra; *middle*: stack of galaxies with Ly-α in emission; *bottom*: stack of galaxies with Ly-α in absorption (this stack is from a subset of the final sample available at the time of writing).

5. Comparison with other spectroscopic surveys at high redshifts

Large spectroscopic surveys at $z > 2$ published in the literature are understandably relatively more limited than surveys at $z < 1.5$ because of the faintness of the sources and because deep imaging requires pre-selection.

We compiled a list, probably not exhaustive, of the main surveys in the redshift range $2 < z < 7$ in Table 5, and we show the corresponding redshift distribution of these surveys in Fig. 24. The largest numbers of galaxies can be found in the range $2 < z < 3$ with the LBG-selected surveys of Steidel et al. (1999, 2003, 2004), the zCOSMOS-Deep survey (Lilly et al. 2007, and in prep.), the VLRS (Bielby et al. 2013), and the VVDS-Deep/Ultra-Deep (Le Fèvre et al. 2013b). In the redshift range $2.5 < z < 3.5$, these surveys accumulate ~2700 galaxies with spectroscopic redshifts. The VUDS survey contributes ~2800 spectroscopic redshifts, which is as much as all these other surveys combined, but in a single well-controled survey.

Beyond redshift $z \sim 3.5$, both the number of spectroscopic surveys and the number of galaxies with measured spectroscopic redshifts decrease dramatically. Spectroscopic campaigns on the GOODS-South area with VIMOS and FORS2 on the VLT have produced about 114 galaxies with redshifts $z \sim 3$–6. The Keck-DEIMOS surveys of Stark et al. (2010) contribute more than 300 galaxies in the range $3 < z < 6.5$. VUDS brings more than 800 new galaxies with spectroscopic redshifts in the range

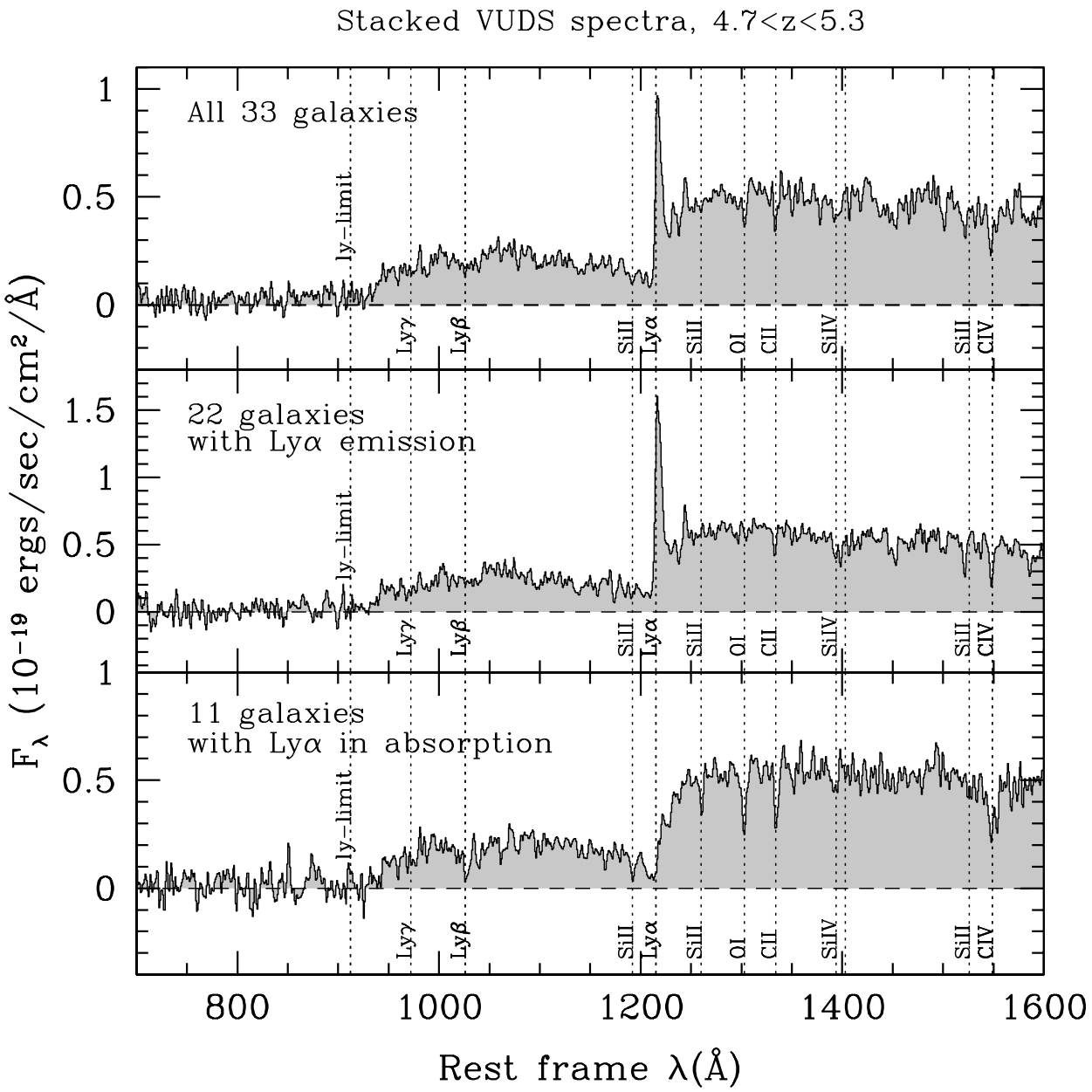

Fig. 22. Average rest-frame spectra (F_λ) of galaxies with flags 2, 3 and 4 in VUDS with $4.7 \leq z \leq 5.3$: *top*: stack of all galaxy spectra; *middle*: stack of galaxies with Ly-α in emission; *bottom*: stack of galaxies with Ly-α in absorption (this stack is from a subset of the final sample available at the time of writing).

$3.5 < z < 5$, or about twice the number of all other surveys combined, as can be seen in Fig. 24.

At the highest redshifts $z > 5$, single redshift confirmations following up on galaxies that are identified as dropout, meaning that they show a sharp change in flux between two adjacent photometric bands (e.g. Stark et al. 2010; Curtis-Lake et al. 2012), following narrow-band LAE candidates (e.g. Ouchi et al. 2010), or serendipitous identification of LAE (Cassata et al. 2011b). These different surveys contribute several tens of spectroscopic identifications beyond $z = 5$. VUDS so far contributes about 60 new sources with spectroscopic redshifts $z > 5$. This sample is being consolidated, particularly at $z > 6$, and will be the subject of future studies.

An important element to keep in perspective is the area sampled by a survey. Fluctuations in number density of objects observed in deep surveys result from the cosmic variance in the distribution of galaxies in large-scale structure. The expected cosmic variance for a given area, redshift, and depth can be computed for example following the prescription of Moster et al. (2011). Surveys with one sq. deg at $z \sim 3$ are subject to an uncertainty of about 10% from cosmic variance, in addition to the uncertainties related to the number of objects in a survey. For fields of the GOODS size (~150 arcmin^2), the cosmic variance at $z \sim 3$ is expected to be in excess of 50% for galaxies with stellar masses $M_* > 10^{10.5}\ M_\odot$.

We compare in Fig. 25 the number of spectra per sq. deg vs. the area for different surveys, a high-redshift version of that presented in Baldry et al. (2010) and updated by Le Fèvre et al. (2013b). While at $z \sim 3$, several surveys have surveyed about 1 sq. deg (Steidel et al. 2003; Lilly et al. 2007; Bielby et al. 2013; Le Fèvre et al. 2013b), the highest redshift surveys at $z > 3$ have only surveyed about 0.1 deg^2 (e.g.

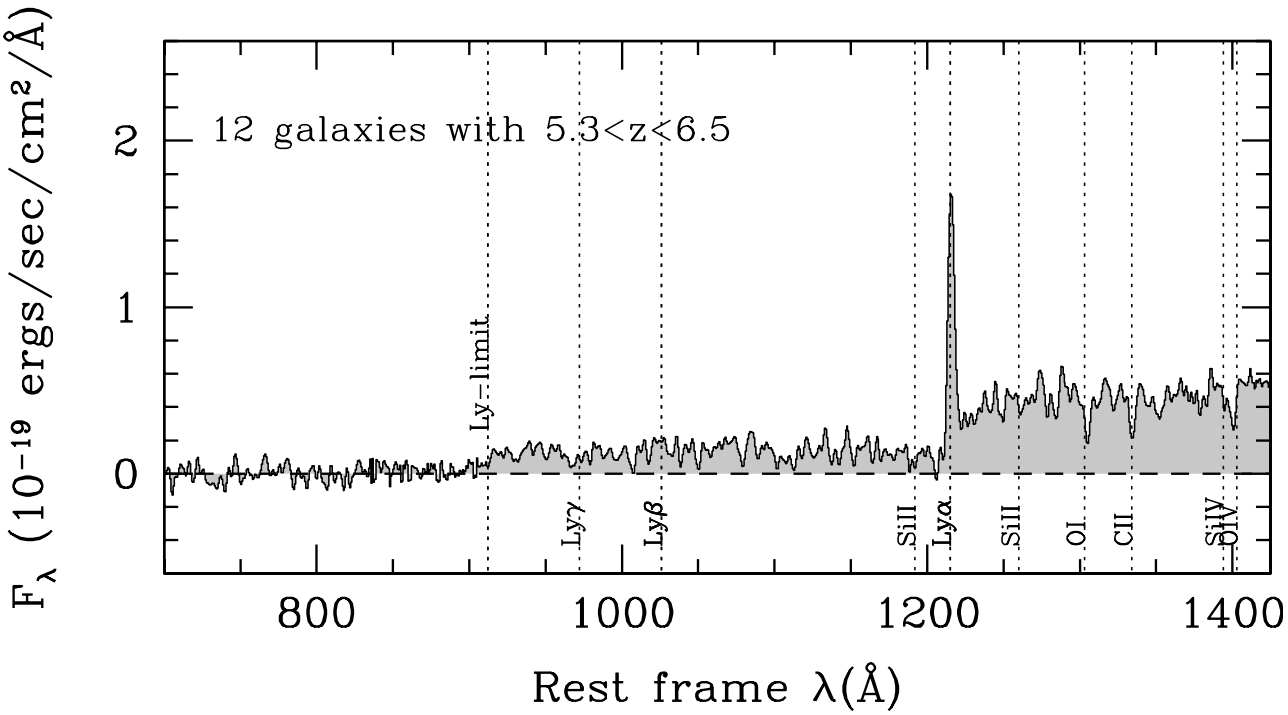

Fig. 23. Average rest-frame spectra (F_λ) of galaxies with flags 2, 3 and 4 in VUDS with $5.3 \leq z \leq 6.5$ (this stack is from a subset of the final sample available at the time of writing).

Table 5. Comparison of the VUDS survey with other spectroscopic redshift surveys at $z > 2$ in the literature, by order of increasing mean redshift.

Survey	Area deg^2	Depth i_{AB} eq.	N_{obj} in Survey	N_{obj} at $z \geq 2$	z_{range}	z_{mean}	Selection	Reference
VVDS-Deep	0.74	24.00	11 601	634	0–5	0.92	$17.5 \leq I_{AB} \leq 24.0$	Le Fèvre et al. (2013)
VVDS-UDeep	0.14	24.75	941	341	0–4.5	1.38	$23.0 \leq i_{AB} \leq 24.75$	Le Fèvre et al. (2014)
Steidel-z2	0.48	$R = 25.5$	851	588	1.4–2.5	2.0	$BM - BX$	Steidel et al. (2004)
zCosmos-Deep	1	23.75	~7500	~4100	1.5–3	2.1	$B_{AB} \leq 25$+colour	Lilly et al. (2007), Lilly et al. (in prep.)
VLRS	1.62	24.7	2135	2135	2–3.5	2.8	$23 < R < 25$	Bielby et al. (2013)
LBG-z3	0.38	24.8	1000		2.7–3.5	3.2	$R_{AB} < 25.5$+colour	Steidel et al. (2003)
GOODS	0.09	$z = 26$	887	114	3	3.5	$(i_{775} - z_{850}) > 0.6, z_{850} < 26$	Vanzella et al. (2009) and Ref. therein
VVDS-LAE	0.74	–	217	217	0–6.7	3.5	$23.0 \leq i_{AB} \leq 24.75$	Cassata et al. (2011)
LBG-z4	0.38	25.0	300	300	3.5–4.5	4.0	$I_{AB} < 25$colour	Steidel et al. (1999)
Dropout-z456	0.09	–	310	310	3–6.5	4.5	Dropout, Lyα break	Stark et al. (2010)
LAE-z6	1	~27	16	16	~6.5	6.5	LAE narrow band	Ouchi et al. (2010)
VUDS	1	25–27	~10 000	~6000[a]	2–6.7	3.0	$i_{AB} < 25$+photo-z	This paper

Notes. [(a)] Adjusted to take into account new data that are not yet processed.

Vanzella et al. 2009; Stark et al. 2010). In this context, VUDS is a unique survey with selected galaxies at any redshift $z > 2$ in three different fields for a total of ~1 deg^2.

6. Summary

The VIMOS Ultra Deep Survey (VUDS) is a deep spectroscopic redshift survey aiming to study the early phases of galaxy assembly at $2 < z < 6.5$ from a sample of ~10 000 galaxies observed with the VIMOS multi-slit spectrograph at the ESO-VLT. The survey target selection is based on photometric redshifts derived from extensive multi-wavelength data for 87.7% of the sample, supplemented by colour–colour diagrams and SED selection for 12.3%. Most of the sample is limited to $i_{AB} = 25$, but galaxies are observed as faint as $i_{AB} = 27$.

The combination of a wide wavelength coverage from 3650 Å to 9350 Å and exposure times of ≃14 h leads to a spectroscopic success rate in redshift measurement of about 91% (74% for spectroscopic reliability flags 2 to 9) down to $i_{AB} = 25$. The comparison of photometric redshifts to the VUDS spectroscopic redshifts shows that the VUDS strategy produces a smaller loss of galaxy populations than more restrictive selection criteria.

We reported on the general properties of the sample based on the ~80% of the data that have already been processed. The redshift distribution of the current sample at $z \geq 2$ peaks at a mean $z = 3$ and extends beyond $z = 6$. A secondary sample at $z < 2$ is the result of the selection function and provides interesting galaxies with a very low intrinsic luminosity. The average spectral properties of galaxies with $z > 2$ were discussed based on

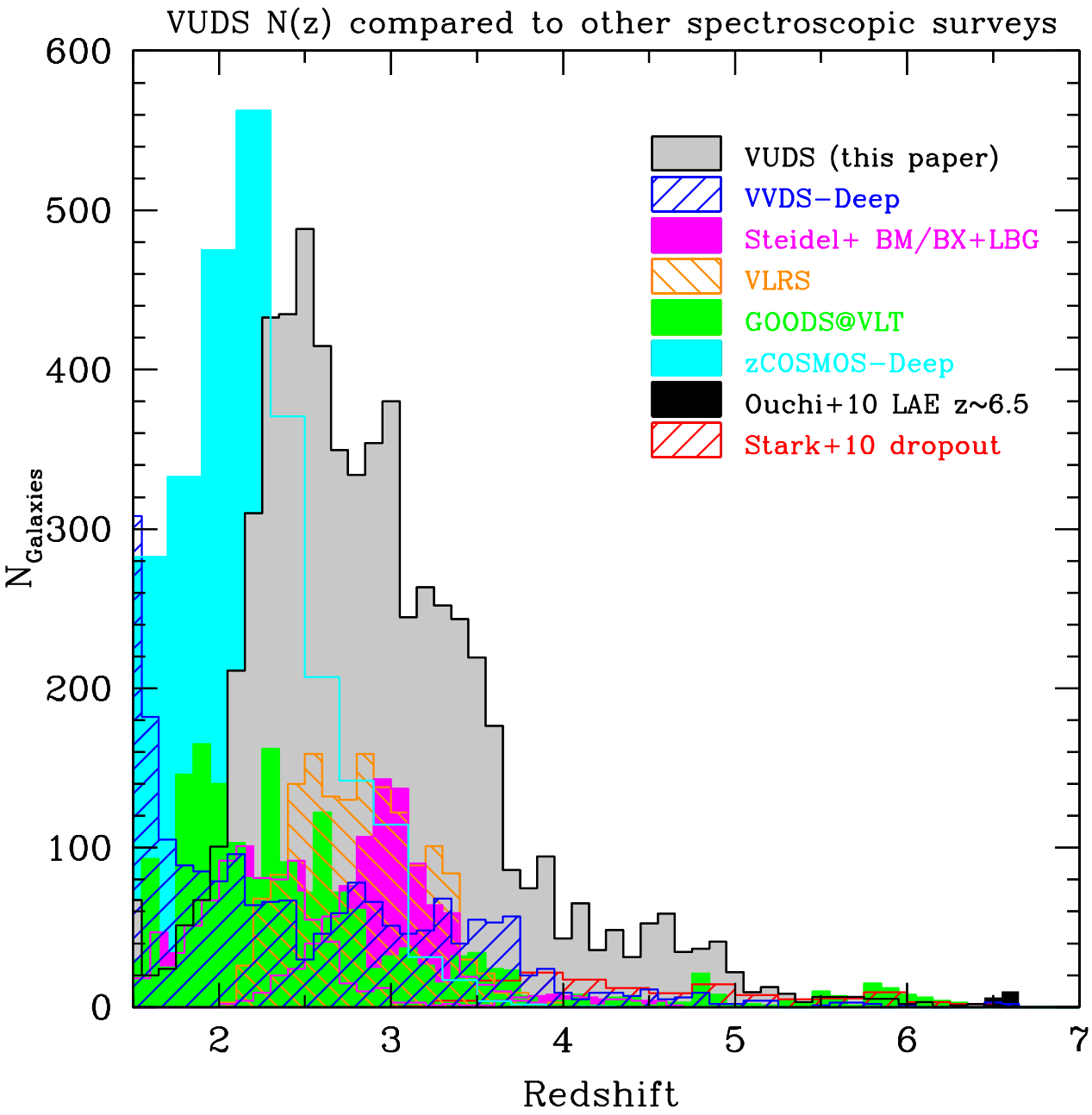

Fig. 24. Comparison of the redshift distribution of the VUDS survey with other published spectroscopic surveys at $z > 2$ (as listed in Table 5). The VUDS counts from existing measurements have been scaled by 1.05 to account for the data not yet processed at the time of writing.

high S/N stacks of VUDS spectra in several increasing redshift bins. Galaxies with and without Lyα in emission are found at any redshift, but we found that the fraction of galaxies with Lyα in emission increases with redshift, as was further quantified in Cassata et al. (2015). Using stacked spectra, we found that there is observed flux below the 912 Å Lyman limit in all explored redshift ranges, the origin of which is currently investigated and will be the subject of future papers.

Following an early measurement of the merger rate at $z \sim 3$ (Tasca et al. 2014b), several papers presenting results from the VUDS are published (Cucciati et al. 2014; Cassata et al. 2015; Lemaux et al. 2014a; Amorín et al. 2014) or submitted (Durkalec et al. 2015, 2014; Tasca et al. 2014a; Thomas et al. 2014). A number of other analyses are in progress.

VUDS is the first deep spectroscopic survey to cover such a wide redshift range with this many galaxies with confirmed spectroscopic redshifts. It is ideally suited for detailed studies of the galaxy population at early times $2 < z < 6$. When the full dataset is completed, we plan on making the VUDS data releases publicly available.

Acknowledgements. We thank the ESO staff for their continuous support for the VUDS survey, particularly the Paranal staff, who conduct the observations, and Marina Rejkuba and the ESO user support group in Garching. This work is supported by funding from the European Research Council Advanced Grant ERC-2010-AdG-268107-EARLY and by INAF Grants PRIN 2010, PRIN 2012 and PICS 2013. A.C., O.C., M.T. and V.S. acknowledge the grant MIUR PRIN 2010–2011. D.M. gratefully acknowledges LAM hospitality during the initial phases of the project. This work is based on data products made available at the CESAM data center, Laboratoire d'Astrophysique de Marseille. This work partly uses

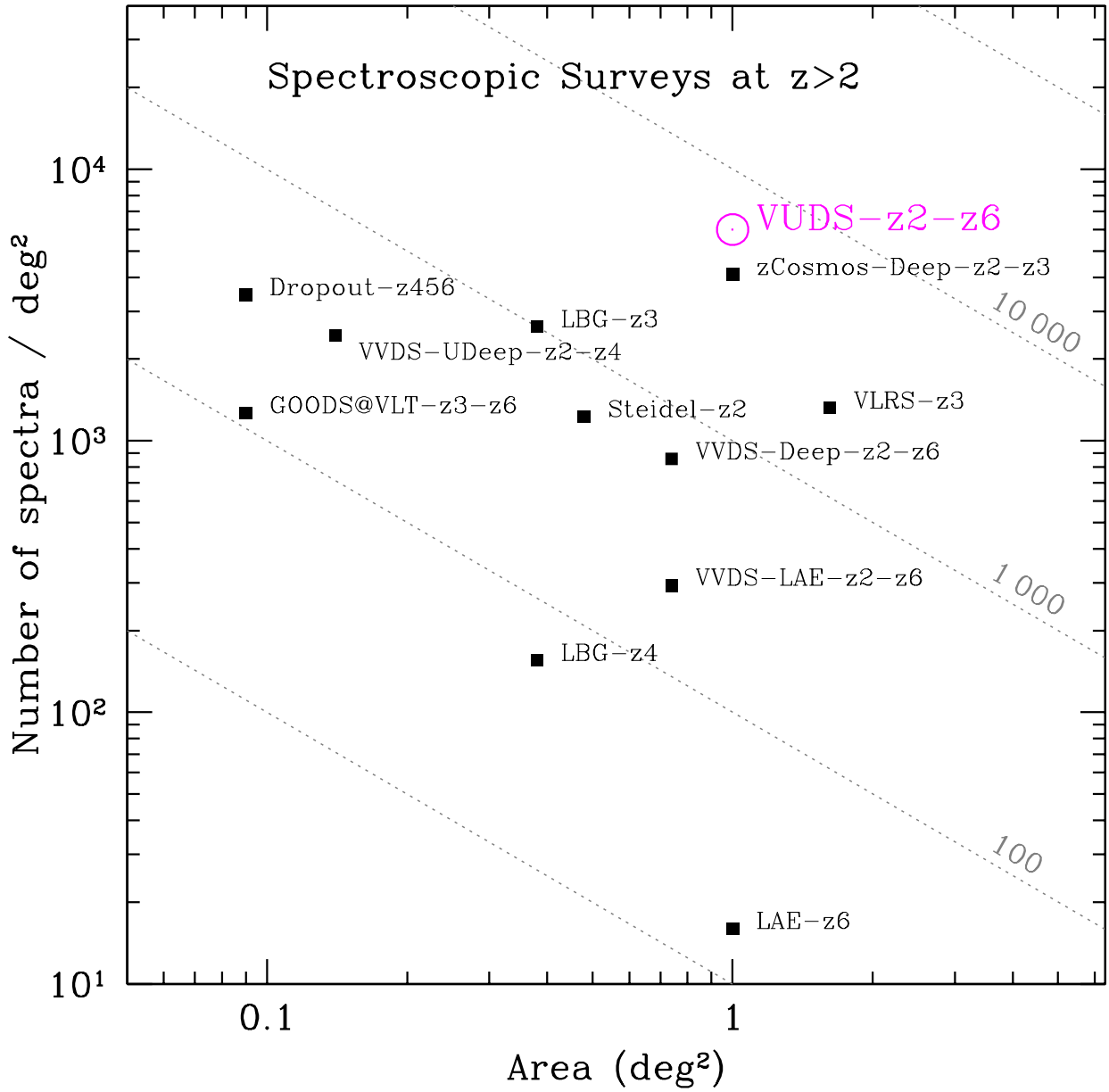

Fig. 25. Comparison of the number density of spectra in the VUDS survey with other published spectroscopic surveys at $z > 2$ (as listed in Table 5). The VUDS counts have been scaled by 1.2 to account for the data not yet processed at the time of writing. Dashed lines are for surveys with a total number of spectra as indicated.

observations obtained with MegaPrime/MegaCam, a joint project of CFHT and CEA/DAPNIA, at the Canada-France-Hawaii Telescope (CFHT) which is operated by the National Research Council (NRC) of Canada, the Institut National des Sciences de l'Univers of the Centre National de la Recherche Scientifique (CNRS) of France, and the University of Hawaii. This work is based in part on data products produced at TERAPIX and the Canadian Astronomy Data Centre as part of the Canada-France-Hawaii Telescope Legacy Survey, a collaborative project of NRC and CNRS.

References

Abazajian, K. N., Adelman-McCarthy, J. K., Agüeros, M. A., et al. 2009, ApJS, 182, 543
Amorín, R., Sommariva, V., Castellano, M., et al. 2014, A&A, 568, L8
Arnouts, S., Cristiani, S., Moscardini, L., et al. 1999, MNRAS, 310, 540
Arnouts, S., Walcher, C. J., Le Fèvre, O., et al. 2007, A&A, 476, 137
Ashby, M. L. N., Willner, S. P., Fazio, G. G., et al. 2013, ApJ, 769, 80
Baldry, I. K., Robotham, A. S. G., Hill, D. T., et al. 2010, MNRAS, 404, 86
Bertin, E., & Arnouts, S. 1996, A&AS, 117, 393
Bielby, R., Hudelot, P., McCracken, H. J., et al. 2012, A&A, 545, A23
Bielby, R., Hill, M. D., Shanks, T., et al. 2013, MNRAS, 430, 425
Bondi, M., Ciliegi, P., Zamorani, G., et al. 2003, A&A, 403, 857
Bottini, D., Garilli, B., Maccagni, D., et al. 2005, PASP, 117, 996
Bouwens, R. J., Illingworth, G. D., Franx, M., et al. 2009, ApJ, 705, 936
Bouwens, R. J., Illingworth, G. D., Oesch, P. A., et al. 2014, ApJ, submitted [arXiv:1403.4295]
Bruzual, G., & Charlot, S. 2003, MNRAS, 344, 1000
Calzetti, D., Armus, L., Bohlin, R. C., et al. 2000, ApJ, 533, 682
Capak, P., Mobasher, B., Scoville, N. Z., et al. 2011, ApJ, 730, 68
Caputi, K. I., Dunlop, J. S., McLure, R. J., et al. 2012, ApJ, 750, L20
Cardamone, C. N., van Dokkum, P. G., Urry, C. M., et al. 2010, ApJS, 189, 270
Cassata, P., Giavalisco, M., Guo, Y., et al. 2011a, ApJ, 743, 96
Cassata, P., Le Fèvre, O., Garilli, B., et al. 2011b, A&A, 525, A143
Cassata, P., Le Fèvre, O., Charlot, S., et al. 2013, A&A, 556, A68
Cassata, P., Tasca, L. A. M., Le Fèvre, O., et al. 2015, A&A, 573, A24
Cimatti, A., Daddi, E., Mignoli, M., et al. 2002, A&A, 381, L68
Cimatti, A., Cassata, P., Pozzetti, L., et al. 2008, A&A, 482, 21
Colless, M., Dalton, G., Maddox, S., et al. 2001, MNRAS, 328, 1039
Cooke, J., Ryan-Weber, E. V., Garel, T., & Díaz, C. G. 2014, MNRAS, 441, 837

Cooper, M. C., Yan, R., Dickinson, M., et al. 2012, MNRAS, 425, 2116
Cucciati, O., Tresse, L., Ilbert, O., et al. 2012, A&A, 539, A31
Cucciati, O., Zamorani, G., Lemaux, B. C., et al. 2014, A&A, 570, A16
Cuillandre, J.-C. J., Withington, K., Hudelot, P., et al. 2012, in Observatory Operations: Strategies, Processes, and Systems IV, SPIE Conf. Ser., 8448
Curtis-Lake, E., McLure, R. J., Pearce, H. J., et al. 2012, MNRAS, 422, 1425
Daddi, E., Cimatti, A., Renzini, A., et al. 2004, ApJ, 617, 746
Davis, M., Faber, S. M., Newman, J., et al. 2003, in Discoveries and Research Prospects from 6- to 10-Meter-Class Telescopes II, ed. P. Guhathakurta, SPIE Conf. Ser., 4834, 161
Durkalec, A., Le Fèvre, O., Pollo, A., et al. 2014, A&A, submitted [arXiv:1411.5688]
Durkalec, A., Le Fèvre, O., de la Torre, S., et al. 2015, 576, L7
Ellis, R. S., McLure, R. J., Dunlop, J. S., et al. 2013, ApJ, 763, L7
Faber, S. M., Phillips, A. C., Kibrick, R. I., et al. 2003, in Instrument Design and Performance for Optical/Infrared Ground-based Telescopes, eds. M. Iye, & A. F. M. Moorwood, SPIE Conf. Ser, 4841, 1657
Garilli, B., Fumana, M., Franzetti, P., et al. 2010, PASP, 122, 827
Giacconi, R., Zirm, A., Wang, J., et al. 2002, ApJS, 139, 369
Grogin, N. A., Kocevski, D. D., Faber, S. M., et al. 2011, ApJS, 197, 35
Guo, Q., White, S., Boylan-Kolchin, M., et al. 2011, MNRAS, 413, 101
Guzzo, L., Scodeggio, M., Garilli, B., et al. 2014, A&A, 566, A108
Hammersley, P., Christensen, L., Dekker, H., et al. 2010, The Messenger, 142, 8
Ilbert, O., Arnouts, S., McCracken, H. J., et al. 2006, A&A, 457, 841
Ilbert, O., Capak, P., Salvato, M., et al. 2009, ApJ, 690, 1236
Ilbert, O., Salvato, M., Le Floc'h, E., et al. 2010, ApJ, 709, 644
Ilbert, O., McCracken, H. J., Le Fèvre, O., et al. 2013, A&A, 556, A55
Kashikawa, N., Shimasaku, K., Matsuda, Y., et al. 2011, ApJ, 734, 119
Koekemoer, A. M., Aussel, H., Calzetti, D., et al. 2007, ApJS, 172, 196
Koekemoer, A. M., Faber, S. M., Ferguson, H. C., et al. 2011, ApJS, 197, 36
Kurk, J., Cimatti, A., Daddi, E., et al. 2013, A&A, 549, A63
Le Fevre, O., Crampton, D., Lilly, S. J., Hammer, F., & Tresse, L. 1995, ApJ, 455, 60
Le Fèvre, O., Saisse, M., Mancini, D., et al. 2003, in Instrument Design and Performance for Optical/Infrared Ground-based Telescopes, eds. M. Iye, & A. F. M. Moorwood, SPIE Conf. Ser., 4841, 1670
Le Fèvre, O., Mellier, Y., McCracken, H. J., et al. 2004a, A&A, 417, 839
Le Fèvre, O., Vettolani, G., Paltani, S., et al. 2004b, A&A, 428, 1043
Le Fèvre, O., Paltani, S., Arnouts, S., et al. 2005a, Nature, 437, 519
Le Fèvre, O., Vettolani, G., Garilli, B., et al. 2005b, A&A, 439, 845
Le Fèvre, O., Cassata, P., Cucciati, O., et al. 2013a, A&A, submitted [arXiv:1307.6518]
Le Fèvre, O., Cassata, P., Cucciati, O., et al. 2013b, A&A, 559, A14
Lemaux, B. C., Cucciati, O., Tasca, L. A. M., et al. 2014a, A&A, 572, A41
Lemaux, B. C., Le Floc'h, E., Le Fèvre, O., et al. 2014b, A&A, 572, A90
Lilly, S. J., Le Fevre, O., Crampton, D., Hammer, F., & Tresse, L. 1995, ApJ, 455, 50
Lilly, S. J., Le Fevre, O., Hammer, F., & Crampton, D. 1996, ApJ, 460, L1
Lilly, S. J., Le Fèvre, O., Renzini, A., & Zamorani, G. 2007, ApJS, 172, 70
Lonsdale, C. J., Smith, H. E., Rowan-Robinson, M., et al. 2003, PASP, 115, 897
Madau, P. 1995, ApJ, 441, 18
Madau, P., & Dickinson, M. 2014, ARA&A, 52, 415
Madau, P., Ferguson, H. C., Dickinson, M. E., et al. 1996, MNRAS, 283, 1388
Mauduit, J.-C., Lacy, M., Farrah, D., et al. 2012, PASP, 124, 714
McCracken, H. J., Milvang-Jensen, B., Dunlop, J., et al. 2012, A&A, 544, A156
Meiksin, A. 2006, MNRAS, 365, 807
Mo, H., van den Bosch, F. C., & White, S. 2010, Galaxy Formation and Evolution (Cambridge University Press)
Moster, B. P., Somerville, R. S., Newman, J. A., & Rix, H.-W. 2011, ApJ, 731, 113
Oliver, S. J., Bock, J., Altieri, B., et al. 2012, MNRAS, 424, 1614
Ouchi, M., Shimasaku, K., Akiyama, M., et al. 2008, ApJS, 176, 301
Ouchi, M., Shimasaku, K., Furusawa, H., et al. 2010, ApJ, 723, 869
Patat, F., Moehler, S., O'Brien, K., et al. 2011, A&A, 527, A91
Pierre, M., Valtchanov, I., Altieri, B., et al. 2004, J. Cosmol. Astropart. Phys., 9, 11
Rix, H.-W., Barden, M., Beckwith, S. V. W., et al. 2004, ApJS, 152, 163
Sanders, D. B., Salvato, M., Aussel, H., et al. 2007, ApJS, 172, 86
Schlegel, D. J., Finkbeiner, D. P., & Davis, M. 1998, ApJ, 500, 525
Scodeggio, M., Franzetti, P., Garilli, B., et al. 2005, PASP, 117, 1284
Scodeggio, M., Franzetti, P., Garilli, B., Le Fèvre, O., & Guzzo, L. 2009, The Messenger, 135, 13
Scoville, N., Aussel, H., Brusa, M., et al. 2007, ApJS, 172, 1
Shapley, A. E., Steidel, C. C., Pettini, M., & Adelberger, K. L. 2003, ApJ, 588, 65
Shapley, A. E., Steidel, C. C., Pettini, M., Adelberger, K. L., & Erb, D. K. 2006, ApJ, 651, 688
Shimasaku, K., Kashikawa, N., Doi, M., et al. 2006, PASJ, 58, 313
Springel, V., Wang, J., Vogelsberger, M., et al. 2008, MNRAS, 391, 1685
Stark, D. P., Ellis, R. S., Chiu, K., Ouchi, M., & Bunker, A. 2010, MNRAS, 408, 1628
Steidel, C. C., Giavalisco, M., Pettini, M., Dickinson, M., & Adelberger, K. L. 1996, ApJ, 462, L17
Steidel, C. C., Adelberger, K. L., Giavalisco, M., Dickinson, M., & Pettini, M. 1999, ApJ, 519, 1
Steidel, C. C., Adelberger, K. L., Shapley, A. E., et al. 2003, ApJ, 592, 728
Steidel, C. C., Shapley, A. E., Pettini, M., et al. 2004, ApJ, 604, 534
Taniguchi, Y., Ajiki, M., Nagao, T., et al. 2005, PASJ, 57, 165
Taniguchi, Y., Scoville, N., Murayama, T., et al. 2007, ApJS, 172, 9
Tasca, L. A. M., Le Fevre, O., Hathi, N. P., et al. 2014a, A&A, submitted [arXiv:1411.5687]
Tasca, L. A. M., Le Fèvre, O., López-Sanjuan, C., et al. 2014b, A&A, 565, A10
Thomas, R., Le Fèvre, O., Cassata, V. L. B. P., et al. 2014, A&A, submitted [arXiv:1411.5692]
Tresse, L., Ilbert, O., Zucca, E., et al. 2007, A&A, 472, 403
Vanzella, E., Giavalisco, M., Dickinson, M., et al. 2009, ApJ, 695, 1163
Vanzella, E., Giavalisco, M., Inoue, A. K., et al. 2010, ApJ, 725, 1011
Wiklind, T., Dickinson, M., Ferguson, H. C., et al. 2008, ApJ, 676, 781
Williams, R. E., Baum, S., Bergeron, L. E., et al. 2000, AJ, 120, 2735
Windhorst, R. A., Cohen, S. H., Hathi, N. P., et al. 2011, ApJS, 193, 27